(19) Europäisches Patentamt
European Patent Office
Office européen des brevets

(11) EP 2 699 165 B1

(12) **EUROPEAN PATENT SPECIFICATION**

(45) Date of publication and mention of the grant of the patent:
07.06.2017 Bulletin 2017/23

(21) Application number: **12774529.7**

(22) Date of filing: **04.01.2012**

(51) Int Cl.:
A61B 5/026 *(2006.01)* ***A61B 17/16*** *(2006.01)*
A61B 17/17 *(2006.01)* ***A61C 1/08*** *(2006.01)*
A61B 5/00 *(2006.01)* ***A61C 19/04*** *(2006.01)*
A61C 8/00 *(2006.01)* ***A61B 5/1455*** *(2006.01)*

(86) International application number:
PCT/IB2012/050045

(87) International publication number:
WO 2012/143798 (26.10.2012 Gazette 2012/43)

(54) **SYSTEM FOR OPTICALLY EVALUATING PROXIMITY TO THE INFERIOR ALVEOLAR NERVE IN SITU**

SYSTEM ZUR OPTISCHEN BESTIMMUNG DER NÄHE ZUM UNTEREN ALVEOLARNERV IN SITU

SYSTÈME POUR ÉVALUER DE MANIÈRE OPTIQUE LA PROXIMITÉ PAR RAPPORT AU NERF ALVÉOLAIRE INFÉRIEUR IN-SITU

(84) Designated Contracting States:
AL AT BE BG CH CY CZ DE DK EE ES FI FR GB GR HR HU IE IS IT LI LT LU LV MC MK MT NL NO PL PT RO RS SE SI SK SM TR

(30) Priority: **21.04.2011 US 201161477787 P**
19.12.2011 US 201113329557

(43) Date of publication of application:
26.02.2014 Bulletin 2014/09

(73) Proprietor: **Live Vue Technologies Inc.**
Ottawa ON K2H 7V5 (CA)

(72) Inventors:
- **MOGHADDAM, Hassan, Ghaderi**
  Ottawa, Ontario K2H 7V5 (CA)
- **GALLANT, Pascal**
  Québec, Québec G2G 2H2 (CA)
- **MERMUT, Ozzy**
  Québec, Québec G2L 3H1 (CA)
- **VEILLEUX, Israël**
  Sainte-Rose-de-Watford
  Québec G0R 4G0 (CA)

(74) Representative: **Lavoix**
Bayerstrasse 83
80335 München (DE)

(56) References cited:
WO-A2-2005/074831
US-A- 6 134 003
US-A1- 2001 047 137
US-A1- 2005 151 976
US-A1- 2006 285 635
US-A1- 2010 280 392
US-B1- 6 419 484
US-B1- 6 485 413
US-B1- 6 564 087

EP 2 699 165 B1

Description

CROSS_REFERENCE TO RELATED APPLICATION

[0001] This application claims priority of US Provisional Patent Application serial number 61/477,787 filed on April 21, 2011 and entitled "METHOD AND SYSTEM FOR OPTICALLY EVALUATING PROXIMITY TO THE INFERIOR ALVEOLAR NERVE IN SITU" and of US Patent Application serial number 13/329,557 filed on December 19, 2011 and entitled "METHOD AND SYSTEM FOR OPTICALLY EVALUATING PROXIMITY TO THE INFERIOR ALVEOLAR NERVE IN SITU".

TECHNICAL FIELD

[0002] The invention relates to methods and systems for evaluating proximity to a target, more specifically, for evaluating proximity to a nerve.

BACKGROUND OF THE ART

[0003] Dental implants are a widely accepted treatment for the partially or completely edentulous patient. Dental implants are the fastest growing procedure in dentistry today. It is a 1 billion dollar industry in the USA. Dental implants offer a suitable alternative to mucosal adhering dentures and allow a more natural option for the patient. Implants have a high success rate when given proper care and when post-surgical instructions are followed. Dental implants can be in the form of a single tooth replacement, or can replace a series or an entire set of teeth. The basic implant procedure involves drilling a channel in the mandible where an artificial root is surgically inserted. A dental prosthesis is then placed onto the frame of the artificial root. Within a few months of recovery, the patient should have a fully integrated and functional prosthesis.

[0004] Implant procedures are not without complications. The goal of an implant procedure is to attain a successful level of osseointegration. Osseointegration is defined as the direct anchorage of an implant by the formation of bony tissue around the implant without the growth of fibrous tissue at the bone-implant interface. Implants surrounded with fibrous tissue show mobility when a load is applied. The successfully osseointegrated implant shows no mobility when loaded. Other major factors for the successful implant depend mainly on the type of jaw treated, the density of the bone, and the length of the implant. Implant length is the depth created by the surgeon upon drilling a channel in the mandible. Short implants have a length of less than 10 mm and are noted to have larger failure rates. Hence the need to create sufficient length for successful osseointegration of implants within the mandible is a priority.

[0005] However, the drilling of a large implant channel within the mandible carries a risk of breaching an intraosseous canal which encloses the inferior alveolar nerve (IAN). Disruption of the IAN can lead to loss of sensation in the anterior mandible area, such as paresthesia or numbness to the lower lip, due to the disruption of the mental nerve, which is the terminal branch of the IAN and is the neural bundle serving this area. The loss of sensation for the patient is certainly undesirable.

[0006] The reported incidence of nerve injury from implant placement in the literature is highly variable and ranges depending on the study from 0% to as high as 44% (Misch and Resnik Implant Dentistry 2010; 19:378-386). A survey at the Misch international institute indicated that 73% of dentists have encountered neurosensory impairment within their practice. To help prevent nerve injury, patients can be subjected to CT scans which are costly and also involve radiation. The standard error for a CT scan is still in the range of 1.7 mm. This measurement error can result in nerve damage.

[0007] There is thus a need to develop a surgical drill which is able to detect the proximity and/or location of the IAN in the mandible, preferably during implant procedures. The sensor device should allow the drill to approach closely, but not impair or damage the IAN within an acceptable error limit of the intraosseous canal. Hence, a system that automatically terminates drill action when in close range of the IAN would be most desirable.

[0008] Document US 2006/0285635 A1 relates to contrast enhanced spectroscopic optical coherence tomography.

[0009] Document US 6,419,484 B1 pertains to an optical coherence tomography guided dental drill.

SUMMARY

[0010] According to the present invention, there is provided a spectral absorption probe system according to claim 1. Preferred embodiments are detailed in the dependent claims.

BRIEF DESCRIPTION OF THE DRAWINGS

[0011] Having thus generally described the nature of the invention, reference will now be made to the accompanying

drawings, showing by way of illustration a preferred embodiment thereof and in which:

FIG. 1 is a sagittal section of a mandible showing the inferior alveolar nerve (IAN) positioned directly underneath the molar teeth;

FIG. 2 is a sagittal section of the inferior alveolar nerve (IAN) positioned at the bottom of the mandible;

FIG. 3 (Prior Art) is a diagram of a standard time-domain Optical Coherence Tomography setup of the prior art;

FIG. 4A (Prior Art) is a diagram of a spatially-encoded Fourier-domain OCT system (SEFD-OCT);

FIG. 4B (Prior Art) is a diagram of a frequency-swept-source-based OCT system, or time-encoded Fourier-Domain OCT system (TEFD-OCT);

FIG. 5 is a schematics of a low coherence interferometry probe system for evaluating proximity to a tissue layer, according to one embodiment.

FIG. 6 is a concept schematics of a drill-integrated IAN sensor based on the NIR spectral absorption technique, according to one embodiment;

FIG. 7 is a schematics of a spectral absorption probe system for evaluating proximity to an artery, according to one embodiment.

FIG. 8 is a graph illustrating impact of propagation in a turbid medium such as biological tissue on an intensity-modulated light beam;

FIG. 9 is a schematics of a heterodyne detection configuration for a IAN sensor, according to one embodiment;

FIG. 10A is a schematics of an embodiment of a standalone IAN proximity sensor handpiece, according to a spectral absorption configuration;

FIG. 10B is a schematics of another embodiment of a standalone IAN proximity sensor handpiece, according to a OCT-based, single fiber configuration;

FIG. 11 is a schematics showing a disjointed spectral absorption IAN sensor configuration, according to one embodiment;

FIG. 12 is a diagram of a double-clad optical fiber-based IAN sensor handpiece design, according to one embodiment;

FIG. 13 is a diagram of a spectral absorption-based IAN sensor apparatus where a pulse oxymeter is used, according to one embodiment;

FIG. 14 is a schematics of another IAN sensor using a conical scanning principle, according to another embodiment;

FIG. 15A is a diagram of a drill-integrated IAN sensor using an optical fiber rotary joint, according to one embodiment;

FIG. 15B is a diagram of a drill-integrated IAN sensor using a non-contact optical coupling, according to another embodiment;

FIG. 16 is a diagram of a one dimensional model of a trabecular bone, according to one embodiment.

FIG. 17 is a flow chart of a probe method for evaluating proximity to a tissue layer, according to one embodiment.

FIG. 18 is a flow chart of a probe method for evaluating proximity to an artery, according to one embodiment.

[0012] It will be noted that throughout the appended drawings, like features are identified by like reference numerals.

DETAILED DESCRIPTION

Anatomy background

[0013] Referring to FIGS. 1 and 2 which show Sagittal sections of a mandible **10**, the inferior alveolar nerve **12** (IAN) is a branch of the mandibular nerve, which stems from the trigeminal nerve system. The IAN **12** enters an intraosseous canal through the mandibular foramen in the posterior portion of the mandible. The nerve continues its path within the mandible **10** and then exits through the mental foramen. Throughout the length of the osseous canal, the IAN **12** is closely associated with the inferior alveolar artery and both structures are covered in a tough sheath of connective tissue. The diameter of the entire bundle varies between patients but averages at 2.53±0.29 mm [C.D. Morris et al., J. Oral Maxillo. Surg., 68:2833-2836, 2010].

[0014] The intraosseous canal is a hollow channel and in most cases has borders with defined walls which may be consistent throughout the length of the canal. The diameter of this canal is known to be 2.0 to 2.6 mm. The canal walls may either be composed of cortical bone, or in lesser frequency, may be continuous and uniform with the surrounding trabecular bone. Many patients have canals which abruptly become uniform and continuous with surrounding cancellous bone within proximity of the mental foramen. Although the intraosseous canal is present in many patients, it is not a consistent feature within the mandibles of every individual. Dissection studies show that cortical walls and distinct osseous canals within mandibles are not always present. Some specimens of IAN were shown to travel the trabecular marrow spaces without any defined canal present.

[0015] The position of the IAN **12** within the mandible **10** is highly variable. In one dissection study, the position of the IAN varied in position from the sub-dental portion below the molar roots (See FIG. 1), to an inferior position near the bottom ridge of the mandible **10** (See FIG. 2). A feature which was not frequent, but was observed, was the splitting of the IAN bundle into diffuse branches without a defined intraosseous canal.

Current IAN Location Methods

[0016] The general imaging methods currently used by surgeons to assess the position of the IAN are Panoramic X-ray, Computed Tomography (CT) scan, and Microradiograph (MR) imaging. As some patients may lack an osseous canal and an IAN bundle altogether, preoperative imaging is imperative. X-rays are usually taken in a panoramic fashion, encircling the entire mandible. This presents a global view of the mandible and images potential implant placement sites. The limitations of this technique are that it provides no information about mandible thickness and suffers from a distortion factor of about 25%. A more modern approach to the imaging of the mandible is the CT scan. This method is able to generate overlapping images through computer software programs. However, for dental surgical purposes, only bone and calcified structures are imaged by CT; the IAN and associated non-osseous tissues are not. Thus the CT scan is limited for patients without defined canal walls; locating the IAN on a single cross section is difficult. Reformatted images of adjacent parallel and perpendicular images must be taken and used to assess the exact relative location of the IAN within the mandible. Detailed X-ray imaging, or Mircoradiograph (MR) imaging, is able to image and provide a notable contrast between osseous and non-osseous tissues. When using MR, the canal is visible in cross-sectional reformations exclusive of the osseous tissue surrounding it. The drawback to using MR imaging is that spatial distortions on MR images may not give proper resolution for smaller distances. This is also true for both CT and Panoramic scans, although the resolution for both these techniques has been shown to be similar. Current CT based technologies are expanding imaging possibilities by integrating novel software and 3-D imaging methods.

[0017] The drawback for all these imaging methods, with the exception of novel 3-D CT scanning methods, is that they are not in real time and must be performed preoperatively before the surgical procedure. These methods are also limited in resolution (typ. ±1.3mm) and may not be able to properly image diffuse IAN layouts for patients without a localized IAN bundle. This adds much uncertainty and leaves the surgeon to estimate the exact locations of the IAN during surgery. Thus, a technology which combines both the procedures of drilling and localization of the IAN into a simultaneous process has yet to be developed.

Machining of Bone and Present Drill Sensor Technology

[0018] In the process of dental implants, drilling is used to create channels within the mandible for the placement of artificial roots.

[0019] The drilling operation performed on the mandible must traverse a cortical bone layer and into a cancellous bone mass. As the drill continues forward, heat is generated at the apex of the drill bit. Some of this heat is absorbed by the surrounding bone, raising its temperature. An implication of temperature rise and heat generation from machining bone is thermal osteonecrosis. Irreversible thermal osteonecrosis occurs when bone temperature reaches and exceeds 47°C. With irreversible osteonecrosis, adequate osseointegration could be inhibited, thus reducing the chances for a

successful implant. When drilling bone without external irrigation, tissue temperatures can range from 31-56°C. An irrigation system is included in most surgical drills for this purpose. Water is injected through an orifice from the apex of the drill bit into the immediate drilling site. This acts to cool the drilling site, and functions to prevent thermal osteonecrosis. For the contribution of heat generation from the drill itself, the most important parameters are drill speed, feed rate and drill diameter. Hence with irrigation, adjustment and control of these parameters can help to reduce heat generation when drilling in bone.

[0020] Currently, drill sensor technology is not aimed at discerning the media situated at the drill-bone interface. Technology is more focused on detecting and imaging wear on drill burs and machinery. There exists drill detection systems aimed at bone machining applications. A mechatronic system developed by Bouazza-Marouf and Ong [Ong, F.R., Bouazza-Marouf, K.; 1999; The detection of drill bit break-through for the enhancement of safety in mechatronic assisted orthopaedic drilling; MECHATRONICS 9: 565-588] is able to discern drill break-through from inherent fluctuations in bone structure when drilling long bones. This system is able to detect differences in force through an electronic logic algorithm. The drawback here is that a certain, constant force is applied and the drill bit feed rate into the bone media is constant. In practice, drilling with constant force and feed rate would not be used due to variability in bony tissues within the body and between patients. The mechatronic system was also not able to discern latent non-osseous tissue. The application of this system for the purpose of long implant placement within the mandible would not be desirable as bone breakthrough is the arresting factor for this system.

Optical-based *in situ* proximity IAN sensor

[0021] Current surgery practice allows for an experienced dental surgeon to drill the mandible down to a distance of 2 mm from the IAN, without too much risk of damaging the nerve bundle. As such, the proximity sensor operating range should be within this 2 mm boundary, although a longer distance of operation would be useful. At the same time, the axial resolution of the sensor should be as high as possible.

[0022] The first approach is based on Low Coherence Interferometry (LCI). A LCI probe can be built to operate in A-mode (i.e. point-scan only, no image). LCI presents similar results to ultrasound echolocation and provides a high-resolution measurement of the tissue layers structure based on back-scattered light intensity from those layers. The measurements being optical in nature, the axial resolution of this technique is at least ten times better than with ultrasound, at the cost of a much lower depth penetration (typ. resolutions in ~10 μm at maximal depths of ~1.5 mm, depending on tissues optical absorption and scattering properties). The particular imaging extension of this technique, i.e B-mode scanning, is known in the art as Optical Coherence Tomography (OCT).

[0023] FIG. 3 shows an embodiment of a standard time-domain LCI or OCT system **30** using a low coherence light source **32** (typically a superluminescent LED or pulsed laser) and an interferometer configuration **34** for performing a longitudinal scanning **36** and a lateral scanning **38**. As illustrated, an optical arrangement **40** is used for implementing the lateral scanning **38** while an optical arrangement **42** comprising a moving mirror **44** is used for implementing the longitudinal scanning **36**. A signal processor **46** may be used in conjunction with a computer **48** for signal processing purposes. Newer designs, as the systems **50** and **52** shown in FIGS. 4A and 4B respectively, involve detecting in the Fourier domain or using frequency-swept light sources to disband with the traditional time-pulsed requirement of the incident light emission. The system **50** comprises a low coherence source (LCS) **54**, an interferometer sub-assembly **56** provided with a beamsplitter (BS) **58** and a reference mirror (REF) **60**. The system **50** also comprises a diffraction grating (DG) **62** and a camera (CAM) **64** for detecting light back-scattered by the sample (SMP) **66**. A digital signal processor (DSP) **68** is operatively connected to the camera **64** for providing an OCT image based on the back-scattered light. The system **52** of FIG. 4B uses a swept source (SS) **72** in place of the low coherence source **54** of FIG. 4A and a photodetector (PD) **70**.

[0024] An A-Mode fibered LCI probe can be designed in a compact form small enough to fit within a dental drill bit, according to one embodiment. Tissue interfaces will appear as an increase in the back-scattered signal intensity. Similarly, in an alternative embodiment, a B-mode 2D image can be generated by building the LCI / OCT probe with an integrated forward-looking proximal or distal scanner, as it should become apparent to the skilled addressee. In the case of the IAN, an interface signal will be generated either by the canal wall or the nerve bundle itself and will be visible in real time to the dental surgeon as long as the interface is within the penetration depth range of the instrument.

[0025] FIG. 5 illustrates a low coherence interferometry probe system **100** for evaluating proximity to a tissue layer **102**, according to the above detailed technique and according to one embodiment. The probe system **100** comprises a low coherence light source **104** for generating low coherence excitation light **106**, an excitation optical fiber **108** to bring the low coherence excitation light **106** near the tissue layer **102** and a collection optical fiber **110** for capturing back-scattered light from the tissue layer **102**. The probe system **100** also comprises a low coherence interferometry sub-system **112** operatively connected to the excitation optical fiber **108** and the collection optical fiber **110** and having a beam splitter **114** and a reference mirror **116**. A digital signal processor **118** operatively connected to the low coherence interferometry sub-system **112** is used for evaluating a distance **120** to the tissue layer **102** based on the back-scattered

light received by the collection optical fiber **110**.

[0026] FIG. 17 illustrates a low coherence interferometry probe method for evaluating proximity to a tissue layer, according to one embodiment. According to processing step **1710**, a low coherence excitation light is generated. According to processing step **1720**, the low coherence excitation light is brought near the tissue layer. According to step **1730**, back-scattered light from the tissue layer is captured. According to processing step **1740**, interferometry between the low coherence excitation light and the back-scattered light is performed for providing an interference signal. According to processing step **1750**, the interference signal is processed for evaluating a distance to the tissue layer.

[0027] Experiments were conducted with a probe system **100** on a post-mortem extracted human jawbone cut in such a way that the LCI entry point surface made a wedge with the approximate location of the canal, thus providing increased depth of the IAN interface with the entry point location. This approach allows to evaluate the depth penetration of the technique. The results indicate a probing range of about 1 mm within the test conditions (ex vivo sample, wavelength of 1.32 μm). An increase in wavelength should improve detection range as tissue scattering decrease monotonically with wavelength. However, one must also fine tune the wavelength so that it fits between tissue absorption lines that are numerous in these ranges due to tissue water content. Appropriate designs for performing LCI / OCT systems seem to favor the use of frequency-swept laser sources for state-of-the-art devices. Availability of such light sources at 1.55 μm is increasing and development at 1.8 μm is ongoing. The skilled addressee will nevertheless appreciate that other arrangements may be considered.

[0028] A second optical approach is to use the spectral absorption properties of arterial blood and the blood flow dynamics (change in blood volume due to the patient's pulse) to measure the distance to this artery based on the Beer-Lambert law of light absorption:

$$I = I_0 \exp(-\mu_{eff} d) \quad [1]$$

where I and I_0 are the detected and incident light intensities, respectively, d is the total propagation distance of the light within tissues (the sensor will measure the distance $s = d/2$) and μ_{eff} is the attenuation coefficient of the medium in which light propagation occurs. In the case of tissues, attenuation is a combination of absorption and scattering of the photons at the illumination wavelength and is tissue-type-dependent.

[0029] A first approximation model can provide an evaluation of the order of magnitude of the return signal. The probing device would operate from within the trabecular bone to identify the artery from the IAN neurovascular bundle. Trabecular bone is a complex structure composed of cortical bone and bone marrow arranged in "cells", similar to a beehive. Optically, this structure may be represented in a one dimensional model **200** where three layers **202**, **204**, **206** are stacked vertically, each representing cortical bone, bone marrow and arterial blood, as illustrated in FIG. 16. In this model, the blood layer thickness varies over time in a periodic fashion to represent the blood volume change in the arteries due to the cardiac cycle. The thickness of the bone and marrow layers is dependent on the porosity of the trabecular structure.

[0030] Using this representation, the equations governing the optical propagation, based on the Beer-Lambert's Law, are:

$$I = I_0 e^{-\left[\mu_{marrow} d_{marrow} + \mu_{cortical} d_{cortical} + \mu_{HbO2}(t) d_{HbO2}(t)\right]} \quad (2),$$

[0031] where μ_x and d_x (x = *marrow, cortical, HbO2*) are the attenuation coefficient and layer thickness of each of the three types of tissue involved. The marrow and cortical layer thicknesses are related to the porosity of the trabecular structure $0 < p < 1$ such that:

$$d_{marrow} = p \text{ X } d_{total}$$

$$d_{cortical} = (1\text{-}p) \text{ X } d_{total} \quad (3),$$

where $d_{total} = d_{marrow} + d_{cortical}$ is the total thickness of trabecular bone between the light input and the arterial layer. Because of blood flow and its properties, the HbO2 terms are time-dependent. Indeed, the distance parameter d_{HbO2} will change due to the volume variation occurring with pulsating blood flow. In the proposed model **200**, this is represented

by a harmonic variation of the thickness of the arterial layer:

$$d_{HbO2}(t) = d_{HbO2-baseline}(1 + \Delta_d \cos(2\pi ft)) \quad (4),$$

where $d_{HbO2\text{-}baseline}$ is the average thickness of the layer, $0 < \Delta_d < 1$ is the maximum fractional thickness change due to pulsating blood flow, t is time and f is the blood pulse frequency in Hz.

[0032] The HbO2 attenuation coefficient should also be considered a time-dependent value as it is related to blood oxygenation levels in the patient, thus dependent on the proportions of oxy- and deoxy-hemoglobin in arterial blood. In practice, however, the variation of blood oxygenation will generally be on a much longer time scale than the variations due to the patient's pulse. Strong and sudden variations of blood oxygenation are rare and indicative of a serious health condition that is unlikely to be encountered in the normal operation of the IAN sensor. Nevertheless, monitoring of blood oxygenation with a pulse oxymeter is considered a good practice in the utilization of such a sensor, if only as a check point for the sensor's calibration, as detailed below. For the sake of the proposed model, the attenuation coefficient was however assumed to be a constant.

[0033] Combining Equs. (2)-(4), the model was built to provide an order of magnitude for the optical signal intensity over time to be expected from such an approach. The resulting output optical power is described with:

$$I(t) = I_0 \exp\left[-\left\{p(\mu_{marrow} - \mu_{cortical}) + \mu_{cortical}\right\}d_{total} - \mu_{HbO2}d_{HbO2-baseline}(1 + \Delta_d \cos(2\pi ft))\right] \quad (5).$$

[0034] The near infrared spectroscopy (NIRS) based sensor goal is to measure the thickness d_{total} of trabecular bone tissue between the probe (or drill) tip and the neurovascular bundle containing the IAN. In one embodiment, a lock-in amplifier may be used to establish the magnitude of the oscillating signal and circumvent the DC signal that is influenced by the static trabecular tissue, as detailed below. In one embodiment, a typical method is to use the root-mean square value of the AC signal:

$$I_{RMS} = \sqrt{\left\langle I^2(t)\right\rangle} \quad (6),$$

where:

$$\left\langle I^2(t)\right\rangle = \int_0^{1/f} t\left[I(t)\right]^2 dt \quad (7).$$

[0035] Solving Equ. (6) from (5) and (7) and using a Taylor expansion for the exponential function up to the second degree in the integral leads to:

$$I_{RMS} \approx \left[\sqrt{2}I_0 \frac{1}{2f}\sqrt{1 + B^2\Delta_d^2}\right]e^{-Kd_{total}+B};$$
$$B = \mu_{HbO2}d_{HbO2-baseline}; \quad (8),$$
$$K = p(\mu_{marrow} - \mu_{cortical}) + \mu_{cortical}$$

and thus,

$$d_{total} \approx \left\{ \mu_{HbO2} d_{HbO2-baseline} - \ln\left(\sqrt{2} f \left(\frac{I_{RMS}}{I_0} \right) \frac{1}{\sqrt{1+(\Delta_d \mu_{HbO2} d_{HbO2-baseline})^2}} \right) \right\} \frac{1}{p(\mu_{marrow} - \mu_{cortical}) + \mu_{cortical}}$$

(9).

[0036] With such a model, assuming an input of 10 mW of optical power at the proper wavelength, an output signal of approximately 0.07 mW would be produced.

[0037] FIG. 7 shows a spectral absorption probe system **300** for evaluating proximity to an artery **302**, according to the above detailed technique and according to one embodiment. The probe system **300** comprises a light source **304** for generating excitation light **306** having a wavelength adapted for absorption by blood chromophores, an excitation optical fiber **308** to bring the excitation light **306** near the artery **302** and a collection optical fiber **310** for capturing back-scattered light from the artery **302**. The probe system **300** comprises a light detector **312** operatively connected to the collection optical fiber **310** and a signal processor **314** operatively connected to the light detector **312** for determining a distance **320** to the artery **302** based on the back-scattered light and on Beer-Lambert law of light absorption using a value for surrounding tissue attenuation coefficient (μeff).

[0038] FIG. 18 illustrates a spectral absorption probe method for evaluating proximity to an artery, according to one embodiment. According to processing step **1810**, an excitation light having a wavelength adapted for absorption by blood chromophores is generated. According to processing step **1820**, the excitation light is brought near the artery. According to processing step **1830**, back-scattered light is captured from the artery. According to processing step **1840**, the back-scattered light from the artery is processed for determining a distance to the artery based on Beer-Lambert law of light absorption using a value for surrounding tissue attenuation coefficient (μeff).

[0039] As anatomically the artery is part of the IAN bundle, locating it is almost equivalent to locating the nerve. This approach can be implemented in a similar package as the LCI / OCT fiber probe that can fit within the dental drill bit. The blood pulse can be used to eliminate all background signals via AC-coupling of the detector or lock-in amplification. The signal amplitude can then be used to assess the distance from the probe to the IAN bundle based on Beer-Lambert's law. A calibration process is however typically required before use *in situ* due to patient's tissues variability of optical properties. Notably, the approach relies on the absorption of oxyhemoglobin, which itself will potentially vary according to blood oxygen saturation. As such, the approach might benefit from the probe being used in conjunction with a pulse oxymeter that would monitor oxygen saturation levels and thus, indirectly account for variations of the blood attenuation coefficient. A variation on this approach uses the same spectral principle as the pulse oxymeter, utilizing two wavelengths (typically, 660 nm to target deoxyhemoglobin and 850 nm to target oxyhemoglobin, but generally comprised between 650 nm and 900 nm), as shown in FIG. 6 which illustrates a drill-integrated IAN sensor **600** based on the NIR spectral absorption technique. As detailed therein, distance can be obtained by isolating the distance variable (d) in Equ. 1, but requires that the surrounding tissues' attenuation coefficient (μeff) be known through a calibration step. It has to be noted that such a technique would be limited in the precision of the measurement, as the signal output results from probing a large volume with diffused photons and is thus inherently averaging over that volume, which might skew the output value of distance. Using AC-coupling and a proper calibration is key in this approach, as detailed thereafter.

[0040] In one embodiment, the calibration for the spectral absorption technique may be integrated within the standard configuration if a lock-in amplifier (not shown) is used. In such an embodiment, as illustrated in FIG. 8, an intensity-modulated light excitation of modulation frequency f (typ. ~100 MHz range) and modulation depth M1 propagating in the tissues will suffer phase retardation and reduction of the modulation depth as a function of the attenuation properties of the traversed medium. The retrieved signal has the same frequency as the incident one, but due to absorption and scattering in the medium, it suffers a phase shift $\Delta\Phi$ and an attenuation of the modulation depth M2 relative to the incident signal. The change in phase $\Delta\Phi$ and modulation depth ΔM is correlated to the average attenuation coefficient and can be used to extract the parameter μ_{eff} in Equ. 1. This method is known in the art of Diffuse Optical Tomography. To achieve accurate results, though, the modulation frequency should be in the range of about 100 MHz to 500 MHz. Unfortunately, limitations in current lock-in amplifier electronics make most affordable conventional devices to operate up to the hundreds of kHz range.

[0041] This issue can be solved by using a heterodyning processing circuit before the lock-in amplifier input, as illustrated in FIG. 9, using signal mixing with an intermediate frequency and using principles of Amplitude Modulation to extract the difference signal. In the illustrated embodiment of a probe system **400**, the light source **402** is driven at high frequency with a light source driver **404**, for example at 200 MHz, to insure adequate resolution on the extracted values $\Delta\Phi$ and ΔM. A local oscillator **406** generates a slightly larger frequency, larger by 50 kHz as a non-limitative example. The oscillator **406** and the driver **404** are phase-locked by a PLL circuit **408**. Mixing those two signals produces the sum

and difference signals (amplitude modulation) and a low-pass filter **410** is used to retain only the difference component. The detection channel **412** operates similarly and a standard, low-bandwidth dual-phase lock-in amplifier **414** can then be used.

[0042] Furthermore, it is known in the art that the positioning of the probe for calibration (in contact or not with tissues and other variants) can skew the calibration measurement. The method might thus need an additional step where the instrument is pre-calibrated with an appropriate optical phantom (not shown) with known attenuation properties supplied with the device, before the in-patient calibration step. This way, a relative value to the phantom properties would be obtained and should be enough for the proper operation of the sensor.

[0043] With such an approach, the calibration of the device for the patient's jaw tissues may be made at the beginning or at an early phase of the drilling process by the surgeon, before enabling the sensor, which is of great advantage.

Embodiments and possible features of the Optical IAN Sensor

[0044] Different embodiments of the Optical IAN probe system can be envisioned for both approaches described above. The following is a short description of each of the potential embodiments and implementations envisioned:

[0045] **Standalone self-contained spectral absorption-based fiber-probe:** FIG. 10A shows an embodiment wherein the sensor is built as a standalone fiber optic device **500** contained within a biocompatible metallic rod **502**. The rod **502** contains two optical fibers **504**, **506** (single- or multimode) along its axial direction. One fiber serves to bring the excitation light within the tissues while the other captures the back-scattered light. Fibers **504**, **506** run parallel to each other and are separated by an adequate distance (1-2 mm) to fit into the hole bored by the dental drill bit (typ. 2 mm dia.). The skilled addressee will appreciate that the separation between the two fibers **504**, **506** should be as large as possible to maximize penetration depth. Indeed, in back-reflected diffuse optical sensing, the depth of penetration is increased with source-detector separation. The skilled addressee will also appreciate that multimode fibers may be employed to increase light throughput in both channels. In this embodiment, the fiber probe itself is connected to the device back-end. As previously mentioned, the excitation fiber is connected to a light source (either LED, laser or other source) or multiple light sources each having an appropriate wavelength for optimized absorption by blood chromophores (mainly oxy- and deoxyhemoglobin). Typical wavelengths are around 660 nm and 850 nm. The light source output could be modulated at a reference frequency in the kHz range. The collection fiber is connected to an appropriate light detector such as a photodiode, an avalanche photodiode (APD), a photomultiplier tube (PMT), a camera or the like. The detector output signal is either AC-coupled or connected to a lock-in amplifier operating at the same reference frequency as the light source modulation. The goal of the modulation signal or the AC-coupling is to reject background signals coming from other tissues than the flowing arterial blood. A variation of this embodiment makes use of a varying input optical power into the tissue to establish the neurovascular bundle position relative to the probe based on an intensity threshold approach, where larger input powers will statistically increase linearly the number of photons reaching larger depths, thus improving the chance of detecting some of these photons that might probe the neurovascular bundle.

[0046] **Standalone self-contained low coherence interferometry-based fiber-probe:** FIG. 10B shows another embodiment similar to the one shown in FIG. 10A in shape but implementing the OCT approach. As illustrated, a single fiber **508** can be used for illumination and collection purposes. Due to the difference in requirements between OCT and the spectral absorption concept, the fiber probe should be made of one or multiple single-mode optical fibers to prevent detrimental dispersion and spatial propagation modes mixing, according to one embodiment. The back-end of the probe utilizes classical OCT configurations, such as time-domain-based, frequency-domain OCT or swept-source-based implementations, as previously detailed. In this embodiment, the back-end is entirely fiberized and uses fiber couplers to connect with the probe itself, as is well-known in the art. In a further embodiment, the probe forward-looking configuration can be implemented for B-mode scanning, by integrating a proximal scanning system installed in the back-end coupled to a bundle of single mode optical fibers, or through a distal scanning mechanism integrated into the probe head itself that would use one single-mode optical fiber.

[0047] **Drill-integrated probe:** Referring again to FIG. 6, any of the described embodiments can be integrated at the center of the drill bit **610** of a dental surgery drill. The center of a dental drill bit **610** can have a hollow core **602** to allow for cooling water to circulate down to the drilling site **604**. The fiber probe can be inserted within this hollow core **602**.

[0048] **Combined OCT / Spectral absorption probe:** Such a combined configuration uses the advantages of each approach. The spectral absorption approach has potentially a greater detection range, while the OCT approach is more straightforward and offer potentially better resolution at short range. A combined sensor probe could thus potentially identify roughly the position of the IAN bundle at a distance with the spectral absorption mode and then switch to an OCT approach when close to the IAN (typ. within 1.5 mm). The sensor construction would require two or three optical fibers grouped in a bundle. A single-mode fiber would bring the excitation light. A second single-mode fiber would be used for OCT light collection, while a third multimode fiber would be used for the spectral absorption mode light collection channel. Alternatively, the single-mode excitation fiber could double-up as the collection fiber for the OCT technique.

[0049] **Spectral absorption fiber probe with disjointed source and collection** channels: FIG. 11 shows an em-

bodiment of a disjointed spectral absorption IAN sensor **700**. In this configuration of the spectral absorption technique, one or multiple excitation optical fibers **702** are positioned on the side of the gum or jawbone **704**, outside of the probe handpiece **706** itself (or the drill bit), while the detection optical fiber **708** is still integrated in the probe handpiece **706**, within the drilling hole **710** in the bone **704**. Such a configuration allows larger separation of the source and collection channels, which will increase depth sensitivity of the technique. Indeed, as previously mentioned, in back-reflected diffuse optical sensing, the depth of penetration is increased with source-detector separation. Alternatively, the source and collection channels can be reversed, with the detection being done laterally on the gum and the illumination being integrated in the drill bit, or probe handpiece. In a further embodiment, using multiple optical fibers built in a linear array may provide refined measurements of the neurovascular bundle's position in the jaw.

[0050] Use of a double-clad optical fiber: FIG. 12 illustrates a double-clad optical fiber-based IAN sensor handpiece **800** which may be used alternatively to the use of two optical fibers in the probe. The core **802** of the double-clad optical fiber **804** is used as the excitation channel to send light into tissues and the first cladding **806** acts as the collection channel. In the OCT approach and in one embodiment, the core **802** is built for single mode propagation. The first clad **806** will typically have a large numerical aperture, making it ideal for light collection. The second clad **808** insure proper waveguide behavior for the first clad **806**. This approach would benefit especially the OCT technique as the separation between core and first cladding would probably be too low for efficient implementation of the spectral absorption technique.

[0051] Combining the spectral absorption probe with a pulse oxymeter in the technique: FIG. 13 shows a spectral absorption-based IAN sensor apparatus **900** that uses an entirely separate pulse oxymeter **902** operatively connected to a finger **904** of the patient as a monitor of blood oxygenation variations over the course of the drilling procedure, to maintain an inline calibration of the arterial blood absorption properties. In other words, this embodiment enables to compensate variations of blood optical properties from the oxygenation levels variation ($\Delta SatO2$) to provide more accurate distance measurements, by updating the device calibration factors in real-time. Indeed, large variations in the optical properties will skew the sensor distance measurement. That being said, normal individuals will generally not see variations in blood oxygenation larger than ~2%, which might well be within the error bar of the distance measurement.

[0052] Developing a B-mode OCT technique using the drill rotation for scanning: FIG. 14 shows a IAN sensor **1000** using a conical scanning principle that uses the drill rotation and a beveled double-clad optical waveguide **1002** that rotates with the drill **1004** in such a way that the source and collection channels would observe the tissues in front of the drill tip slightly off-axis. As it should become apparent to the skilled addressee, this is an alternative implementation to the standard B-mode scanning technique that operates along a line in the transverse plane. The drill rotation would allow a ring in the transverse plane to be scanned along the light propagation axis, essentially probing a conical surface within the jaw. The IAN bundle would intersect this conical surface at two opposite locations. The signal processor (not shown) of the device **1000** could then create an image **1006** by "unfolding" the conical surface on a computer screen **1008**, giving the dental surgeon a high resolution image similar to an ultrasonogram in real-time. The advantage of this B-mode scanning method is that the IAN bundle orientation in the transverse plane relative to the drill axis can be arbitrary. In the other implementations described, the IAN bundle should lie on the drilling axis, or the axis of the forward looking probe, to be detected properly. Otherwise the drill bit might pass beside the nerve and still produce damage, because the sensor did not "see" the IAN bundle. Note that with the NIR spectral absorption technique, this flaw is fairly reduced due to the volume averaging effect mentioned earlier.

[0053] Implement Doppler OCT in the probe and use tissue changes or movement as a contrast mechanism: In addition to using standard OCT in the sensor, this configuration uses the Doppler effect to lock on blood flow. Doppler OCT is generally used to measure quantitatively microvasculature blood flow. In the case of this sensor, a qualitative measurement is enough to locate the IAN bundle. As such, the implementation of Doppler measurements in the OCT device would be simpler and cheaper. Experiments were conducted with Doppler OCT on an ex vivo human jawbone piece from which the neurovascular bundle was removed and a tube containing a flowing scattering fluid was connected, imitating blood flow in the canal. Results have shown that using the Doppler Effect as part of the spectral absorption technique might benefit the device.

[0054] According to another embodiment, another variant of OCT data processing that utilizes changes or movement in the tissue like Doppler OCT, namely speckle variance OCT [Refs: A. Mariampillai et al., Opt. Lett. 33(13), 1530 (2008) ; A. Mariampillai et al., Opt. Lett. 35(8), 1257 (2010)], can be used to embody the sensor. It proceeds as follow: first, a series of B-mode images of the same sample section over time is acquired. Second, for each pixel location the average value and variance are computed using pixel value of all images at that same exact location. This process leads to two 2D images. The first one is made with the pixel average value. Therefore, non-zero pixels in that image are those associated with a stationary/non-moving part of the sample. The second image is made with the pixel variance values. Thus, non-zero pixels in that image are associated with the moving/spatially-varying part of the sample. In a similar fashion to Doppler OCT, this kind of processing will lead to contrast generation between hard and soft tissues in movement, or contrast based on tissue "viscosity". Results have shown that the fluid may be identified from the variance image, contrasting with the bone section. This method could potentially make good usage of blood flow in the neurovascular

bundle.

[0055] **Use of a non-specific vascular contrast agent to facilitate artery detection:** A vascular contrast agent, such as Indocyanine Green which is a NIR fluorescent dye approved for clinical use in a number of indications, can be used to enhance the signal coming from the artery in the IAN bundle. Injection of a bolus of ICG into the systemic circulation will momentarily make the artery in the IAN bundle fluoresce at 830 nm (when excited at 780 nm) against a non-fluorescent background, increasing the overall contrast dramatically. If tuned to the fluorescent wavelength, the spectral absorption sensor technique will have a much easier time at spotting the IAN bundle. The modulated excitation would equally translate to a modulated fluorescence signal. A difficulty is however that the device needs to be calibrated at two wavelengths (780 and 830 nm) instead of one. This can be solved by adding a second light source and operating in the same manner as described above for calibration at the two wavelengths, before the ICG injection.

[0056] In similar fashion, the various embodiments based on LCI / OCT can benefit from the potential application of optical clearing agents at the site of probing. Biocompatible optical clearing agents, such as fructose, glycerol, propylene glycol, glucose or mannitol solutions can partially replace the interstitial fluid due to hyperosmotic properties and provide a refractive index matching medium that reduces scattering due to a number of cell structures and organelles, thus increasing the transparency of the tissues to optical wavelengths and improving the depth penetration.

Dental Drill integration of the Optical IAN Sensor

[0057] Integration of the sensor into a drill bit presents a number of mechanical challenges, the most important ones being the rotation speed and how to protect the optical sensor at the drill tip, without blocking light injection and detection. Dental drills can rotate at rates up to 20,000 RPM. In typical use for dental implant surgery, the rotation speed will be in the range of 2,000 to 4,000 RPM.

[0058] To fit within the hollow core of a drill bit, the optical fiber assembly should be secured in such a way that the optical fibers do not come into contact with the rotating inner wall. The friction at high rotating speeds would most certainly break the optical fibers. An alternative is to have the fiber assembly rotate with the drill bit, so that relative positioning of the fibers and the inner wall is stationary. FIG. 15A shows a drill-integrated IAN sensor **1100** rotating with the drill bit **1102** and using an optical fiber rotary joint **1104** for coupling the optical fibers in the drill head.

[0059] FIG. 15B illustrates another alternative drill integrated IAN sensor **1150** wherein a rod-like optical waveguide **1152** is built as an integral part of the drill bit **1154** with a non-contact optical coupler **1156** from the optical fibers **1158** coming from the back-end in the drill head. The skilled addressee will note that having a rotating handpiece requires that the probe design have circular symmetry, which is not achievable with a two-fiber design as the one shown in FIG. 10A. In this last case, the handpiece should remain stationary with the drill bit rotating around the sensing assembly, as previously detailed.

[0060] In a further embodiment, in order to prevent introduction of organic tissues and debris within the hollow core that could clog it and prevent proper function of the sensor, the tip of the drill bit may be plugged with a hard and transparent material (not shown), so it can withstand the large frictions of the drilling process while allowing light to pass through. Diamond or zirconium crystals would potentially be the best materials, due to their exceptional hardness and transparency in the visible and NIR spectral window but the skilled addressee will appreciate that other arrangements may be considered.

Extensions of the technology to other applications

[0061] The described invention could also be used in other fields of surgery where proximity to a neurovascular bundle embedded in hard tissues, such as bone, must be assessed during a surgical activity such as drilling or cutting. It can also be used to identify the presence of voids inside tissue structures, such as sinus cavities in the cranial anatomy, during drilling procedures. As another example of application, a LCI / OCT-based probe could also be envisioned as a bone mapping tool in oral surgery to determine the gums thickness at specific locations, as long as the device detection range is sufficient.

[0062] The embodiments described above are intended to be exemplary only. The scope of the invention is therefore intended to be limited solely by the appended claims.

Claims

1. A spectral absorption probe system (300) using the spectral absorption properties of arterial blood and the blood flow dynamics, that is the change in blood volume in an artery due to a patient's pulse, for evaluating proximity to the artery (302), comprising:

a light source (304) for generating excitation light (306) having a wavelength adapted for absorption by blood chromophores;
an excitation optical fiber (308) to bring said excitation light near the artery;
a collection optical fiber (310) separated from the excitation optical fiber (308) for capturing back-scattered light from said artery;
a light detector (312) operatively connected to said collection optical fiber; and
a signal processor (314) operatively connected to said light detector for determining a distance (320) to said artery based on said back-scattered light and on Beer-Lambert law of light absorption using a time dependent value for surrounding tissue attenuation coefficient (μeff).

2. The spectral absorption probe system (300) as claimed in claim 1, further comprising a biocompatible metallic rod (502) surrounding said excitation optical fiber and said collection optical fiber.

3. The spectral absorption probe system (300) as claimed in claim 1, wherein said excitation optical fiber (308) and said collection optical fiber (310) are provided in a single double-clad optical fiber (804) with a fiber core (802) of said double-clad optical fiber bringing said excitation light near said artery and a first clad of said double-clad optical fiber capturing said back-scattered light from said artery.

4. The spectral absorption probe system (300) as claimed in any one of claims 1 to 3, wherein said probe system is fibered and integrated within a hollow core (602) of a drill bit (610).

5. The spectral absorption probe system (300) as claimed in any one of claims 1 to 4, wherein an operating depth range of the probe system is comprised between 1 mm and 5 mm.

6. The spectral absorption probe system (300) as claimed in any one of claims 1 to 5, wherein the light source (304) is selected from a group consisting of a LED, a laser and a set of light source units, wherein the wavelength of the light source is comprised between 650 nm and 900 nm.

7. The spectral absorption probe system (300) as claimed in any one of claims 1 to 6, further comprising an additional light source having a wavelength adapted for absorption by blood chromophores, the wavelengths of the light source and of the additional light source being each comprised between 650 nm and 900 nm.

8. The spectral absorption probe system (300) as claimed in any one of claims 1 to 7, wherein the light detector (312) is selected from a group consisting of a photodiode, an avalanche photodiode (APD), a photomultiplier tube (PMT) and a camera.

9. The spectral absorption probe system (300) as claimed in any one of claims 1 to 8, further comprising a calibration unit having a pulse oxymeter (902) for monitoring oxygen saturation levels to maintain an inline calibration of arterial blood absorption properties.

10. The spectral absorption probe system (300) as claimed in any one of claims 1 to 9, wherein said surrounding tissue attenuation coefficient (μeff) is determined according to absorption and scattering in surrounding tissue of a calibration excitation signal.

11. The spectral absorption probe system (300) as claimed in any one of claims 1 to 10, wherein the signal processor (314) comprises a lock-in amplifier and a heterodyning processing circuit connected thereto and/or wherein the light detector (312) is AC-coupled to the signal processor.

12. The spectral absorption probe system (300) as claimed in any one of the previous claims, wherein a single one of said excitation optical fiber (308) and said collection optical fiber (310) is integrated within a hollow core of a drill bit.

13. The spectral absorption probe system (300) as claimed in any one of claims 1 to 12, wherein said light source (304) has low coherence, and further comprising:

a low coherence interferometry sub-system (112) operatively connected to the excitation optical fiber and the collection optical fiber and having a beam splitter (114) and a reference mirror (116); and
a signal processor (118) operatively connected to said low coherence interferometry sub-system for evaluating a distance to said artery based on said back-scattered light received by said collection optical fiber.

14. The spectral absorption and low coherence interferometry probe system as claimed in claim 13, wherein the excitation optical fiber (308) comprises a single mode fiber and further wherein the collection optical fiber comprises a single mode fiber for OCT mode light collection and a multimode fiber for spectral absorption mode light collection.

15. The spectral absorption and low coherence interferometry probe system as claimed in any one of claims 13 and 14, wherein the probe system comprises a forward-looking transverse scanner enabling B-mode imaging.

Patentansprüche

1. Sondensystem zur spektralen Absorption (300), das die Eigenschaften der spektralen Absorption von arteriellem Blut und die zeitabhängige Blutflussdynamik, d.h. die Veränderung des Blutvolumens in der Arterie auf Grund des Pulses eines Patienten, verwendet, um die Nähe zur Arterie (302) zu bewerten, umfassend:

   eine Lichtquelle (304) zum Generieren eines Erregerlichts (306), das eine Wellenlänge aufweist, die zur Absorption durch Blutchromophore geeignet ist;
   eine Erregerlichtleitfaser (308), um das Erregerlicht nahe an die Arterie zu bringen;
   eine Sammellichtleitfaser (310), die von der Erregerlichtleitfaser (308) getrennt ist, um das Licht aufzufangen, das von der Arterie zurückgestreut wird;
   einen Photodetektor (312), der funktionsfähig mit der Sammellichtleitfaser verbunden ist, um ein Schwingungssignal zu generieren, das sich im Verlauf der Zeit periodisch ändert, um die Veränderung des Blutvolumens in der Arterie auf Grund des Herzzyklus darzustellen; und
   einen Signalprozessor (314), der funktionsfähig mit dem Photodetektor verbunden ist, um eine Entfernung (320) bis zu der Arterie basierend auf dem zurückgestreuten Licht und dem Lambert-beerschen Gesetz der Lichtabsorption unter Verwendung einer Amplitude des Schwingungssignals und eines Wertes für einen Schwächungskoeffizienten (μeff) des umgebenden Gewebes zu bestimmen.

2. Sondensystem zur spektralen Absorption (300) nach Anspruch 1, ferner umfassend einen Stab (502) aus körperverträglichem Metall, der die Erregerlichtleitfaser und die Sammellichtleitfaser umgibt.

3. Sondensystem zur spektralen Absorption (300) nach Anspruch 1, wobei die Erregerlichtleitfaser (308) und die Sammellichtleitfaser (310) in einer einzigen doppelt ummantelten Lichtleitfaser (804) bereitgestellt werden, wobei ein Faserkern (802) der doppelt ummantelten Lichtleitfaser das Erregerlicht der Arterie nähert, und erster Mantel der doppelt ummantelten Lichtleitfaser das von der Arterie zurückgestreute Licht auffängt.

4. Sondensystem zur spektralen Absorption (300) nach einem der Ansprüche 1 bis 3, wobei das Sondensystem mit Fasern ausgestattet ist und im Innern eines hohlen Kerns (602) eines Bohrers (610) integriert ist.

5. Sondensystem zur spektralen Absorption (300) nach einem der Ansprüche 1 bis 4, wobei ein Betriebstiefenbereich des Sondensystems zwischen 1 mm und 5 mm liegt.

6. Sondensystem zur spektralen Absorption (300) nach einem der Ansprüche 1 bis 5, wobei die Lichtquelle (304) aus einer Gruppe ausgewählt wird, die aus einer LED, einem Laser und einem Satz von Lichtquelleneinheiten besteht, wobei die Wellenlänge der Lichtquelle zwischen 650 nm und 900 nm liegt.

7. Sondensystem zur spektralen Absorption (300) nach einem der Ansprüche 1 bis 6, ferner umfassend eine zusätzliche Lichtquelle, die eine Wellenlänge aufweist, die für eine Absorption durch Blutchromophore geeignet ist, wobei die Wellenlängen der Lichtquelle und der zusätzlichen Lichtquelle jeweils zwischen 650 nm und 900 nm liegen.

8. Sondensystem zur spektralen Absorption (300) nach einem der Ansprüche 1 bis 7, wobei der Photodetektor (312) aus einer Gruppe ausgewählt wird, die aus einer Photodiode, einer Lawinen-Photodiode (APD), einer Photovervielfacherröhre (PMT) und einer Kamera besteht.

9. Sondensystem zur spektralen Absorption (300) nach einem der Ansprüche 1 bis 8, ferner umfassend eine Kalibriereinheit, die ein Pulsoximeter (902) zum Überwachen von Sauerstoffsättigungspegeln aufweist, um eine Inline-Kalibrierung der Absorptionseigenschaften des arteriellen Bluts zu bewahren.

10. Sondensystem zur spektralen Absorption (300) nach einem der Ansprüche 1 bis 9, wobei der Schwächungskoef-

fizient (μeff) des umgebenden Gewebes je nach der Absorption und der Streuung in dem umgebenden Gewebe eines Erregersignals der Kalibrierung bestimmt wird.

11. Sondensystem zur spektralen Absorption (300) nach einem der Ansprüche 1 bis 10, wobei der Signalprozessor (314) einen Lock-in-Verstärker und eine Überlagerungsverarbeitungsschaltung, die daran angeschlossen ist, umfasst, und/oder wobei der Photodetektor (312) mit dem Signalprozessor AC-gekoppelt ist.

12. Sondensystem zur spektralen Absorption (300) nach einem der vorhergehenden Ansprüche, wobei nur eine von der Erregerlichtleitfaser (308) und der Sammellichtleitfaser (310) in einen hohlen Kern eines Bohrers integriert ist.

13. Sondensystem zur spektralen Absorption (300) nach einem der Ansprüche 1 bis 12, wobei die Lichtquelle (304) eine geringe Kohärenz aufweist und ferner Folgendes umfasst:

eine Baugruppe zur Interferometrie mit geringer Kohärenz (112), die funktionsfähig mit der Erregerlichtleitfaser und der Sammellichtleitfaser verbunden ist und einen Strahlenteiler (114) und einen Referenzspiegel (116) umfasst; und
einen Signalprozessor (118), der funktionsfähig mit der Baugruppe zur Interferometrie mit geringer Kohärenz (112) verbunden ist, um eine Entfernung zur Arterie auf der Grundlage des zurückgestreuten Lichts, das von der Sammellichtleitfaser empfangen wird, zu bewerten.

14. Sondensystem zur spektralen Absorption und Interferometrie mit geringer Kohärenz nach Anspruch 13, wobei die Erregerlichtleitfaser (308) eine monomodale Faser umfasst, und wobei ferner die Sammellichtleitfaser eine monomodale Faser umfasst, um Licht im OCT-Modus zu sammeln, und eine multimodale Faser umfasst, um Licht im spektralen Absorptionsmodus zu sammeln.

15. Sondensystem zur spektralen Absorption und Interferometrie mit geringer Kohärenz nach einem der Ansprüche 13 und 14, wobei das Sondensystem einen Vorwärtsquerscanner umfasst, der eine B-Modus-Bildgebung ermöglicht.

Revendications

1. Système de sonde d'absorption spectrale (300) utilisant les propriétés d'absorption spectrale du sang artériel et la dynamique du débit sanguin en fonction du temps, c'est-à-dire la modification du volume sanguin dans l'artère en raison du pouls d'un patient, afin d'évaluer la proximité de l'artère (302), comprenant :

une source de lumière (304) pour générer une lumière d'excitation (306) ayant une longueur d'onde adaptée à l'absorption par des chromophores du sang ;
une fibre optique d'excitation (308) pour rapprocher ladite lumière d'excitation de l'artère ;
une fibre optique collectrice (310) séparée de la fibre optique d'excitation (308) pour capter la lumière rétrodiffusée par ladite artère ;
un détecteur de lumière (312) relié de manière opérationnelle à ladite fibre optique collectrice pour générer un signal oscillant variant dans le temps de manière périodique pour représenter la modification du volume sanguin dans l'artère en raison du cycle cardiaque ; et
un processeur de signal (314) relié de manière opérationnelle audit détecteur de lumière pour déterminer une distance (320) de ladite artère sur la base de ladite lumière rétrodiffusée et la loi de Beer-Lambert de l'absorption de lumière en utilisant une amplitude dudit signal oscillant et une valeur pour un coefficient d'atténuation (μeff) du tissu environnant.

2. Système de sonde d'absorption spectrale (300) selon la revendication 1, comprenant en outre une tige métallique biocompatible (502) entourant ladite fibre optique d'excitation et ladite fibre optique collectrice.

3. Système de sonde d'absorption spectrale (300) selon la revendication 1, dans lequel ladite fibre optique d'excitation (308) et ladite fibre optique collectrice (310) sont fournies dans une seule fibre optique double gaine (804), un coeur de fibre (802) de ladite fibre optique double gaine rapprochant ladite lumière d'excitation de ladite artère et une première gaine de ladite fibre optique double gaine captant ladite lumière rétrodiffusée par ladite artère.

4. Système de sonde d'absorption spectrale (300) selon l'une quelconque des revendications 1 à 3, dans lequel ledit système de sonde est équipé de fibres et intégré à l'intérieur d'un noyau creux (602) d'une mèche (610).

5. Système de sonde d'absorption spectrale (300) selon l'une quelconque des revendications 1 à 4, dans lequel une plage de profondeur de fonctionnement du système de sonde est comprise entre 1 mm et 5 mm.

6. Système de sonde d'absorption spectrale (300) selon l'une quelconque des revendications 1 à 5, dans lequel la source de lumière (304) est sélectionnée dans un groupe composé d'une LED, d'un laser et d'un ensemble d'unités de source de lumière, la longueur d'onde de la source de lumière étant comprise entre 650 nm et 900 nm.

7. Système de sonde d'absorption spectrale (300) selon l'une quelconque des revendications 1 à 6, comprenant en outre une source de lumière supplémentaire ayant une longueur d'onde adaptée pour une absorption par des chromophores sanguins, les longueurs d'onde de la source de lumière et de la source de lumière supplémentaire étant chacune comprise entre 650 nm et 900 nm.

8. Système de sonde d'absorption spectrale (300) selon l'une quelconque des revendications 1 à 7, dans lequel le détecteur de lumière (312) est sélectionné dans un groupe composé d'une photodiode, d'une photodiode à avalanche (APD), d'un tube photomultiplicateur (PMT) et d'une caméra.

9. Système de sonde d'absorption spectrale (300) selon l'une quelconque des revendications 1 à 8, comprenant en outre une unité de calibrage comportant un oxymètre de pouls (902) pour surveiller les taux de saturation en oxygène pour maintenir un calibrage en ligne des propriétés d'absorption du sang artériel.

10. Système de sonde d'absorption spectrale (300) selon l'une quelconque des revendications 1 à 9, dans lequel ledit coefficient d'atténuation (μeff) du tissu environnant est déterminé selon l'absorption et la diffusion d'un signal d'excitation de calibrage dans le tissu environnant.

11. Système de sonde d'absorption spectrale (300) selon l'une quelconque des revendications 1 à 10, dans lequel le processeur de signal (314) comprend un amplificateur synchrone et un circuit de traitement hétérodyne connecté à celui-ci, et/ou dans lequel le détecteur de lumière (312) est couplé au processeur de signal en courant alternatif.

12. Système de sonde d'absorption spectrale (300) selon l'une quelconque des revendications précédentes, dans lequel une seule de ladite fibre optique d'excitation (308) et de ladite fibre optique collectrice (310) est intégrée dans un noyau creux d'une mèche.

13. Système de sonde d'absorption spectrale (300) selon l'une quelconque des revendications 1 à 12, dans lequel ladite source de lumière (304) présente une faible cohérence, et comprenant en outre :

un sous-ensemble d'interférométrie à faible cohérence (112) relié de manière opérationnelle à la fibre optique d'excitation et à la fibre optique collectrice et présentant un séparateur de faisceau (114) et un miroir de référence (116) ; et
un processeur de signal (118) relié de manière opérationnelle audit sous-ensemble d'interférométrie à faible cohérence pour évaluer une distance de ladite artère sur la base de ladite lumière rétrodiffusée reçue par ladite fibre optique collectrice.

14. Système de sonde d'absorption spectrale et d'interférométrie à faible cohérence selon la revendication 13, dans lequel la fibre optique d'excitation (308) comprend une fibre monomodale, et dans lequel la fibre optique collectrice comprend en outre une fibre monomodale pour collecter de la lumière en mode OCT et une fibre multimodale pour collecter de la lumière en mode d'absorption spectrale.

15. Système de sonde d'absorption spectrale et d'interférométrie à faible cohérence selon l'une quelconque des revendications 13 et 14, dans lequel le système de sonde comprend un scanner transversal frontal permettant une imagerie en mode B.

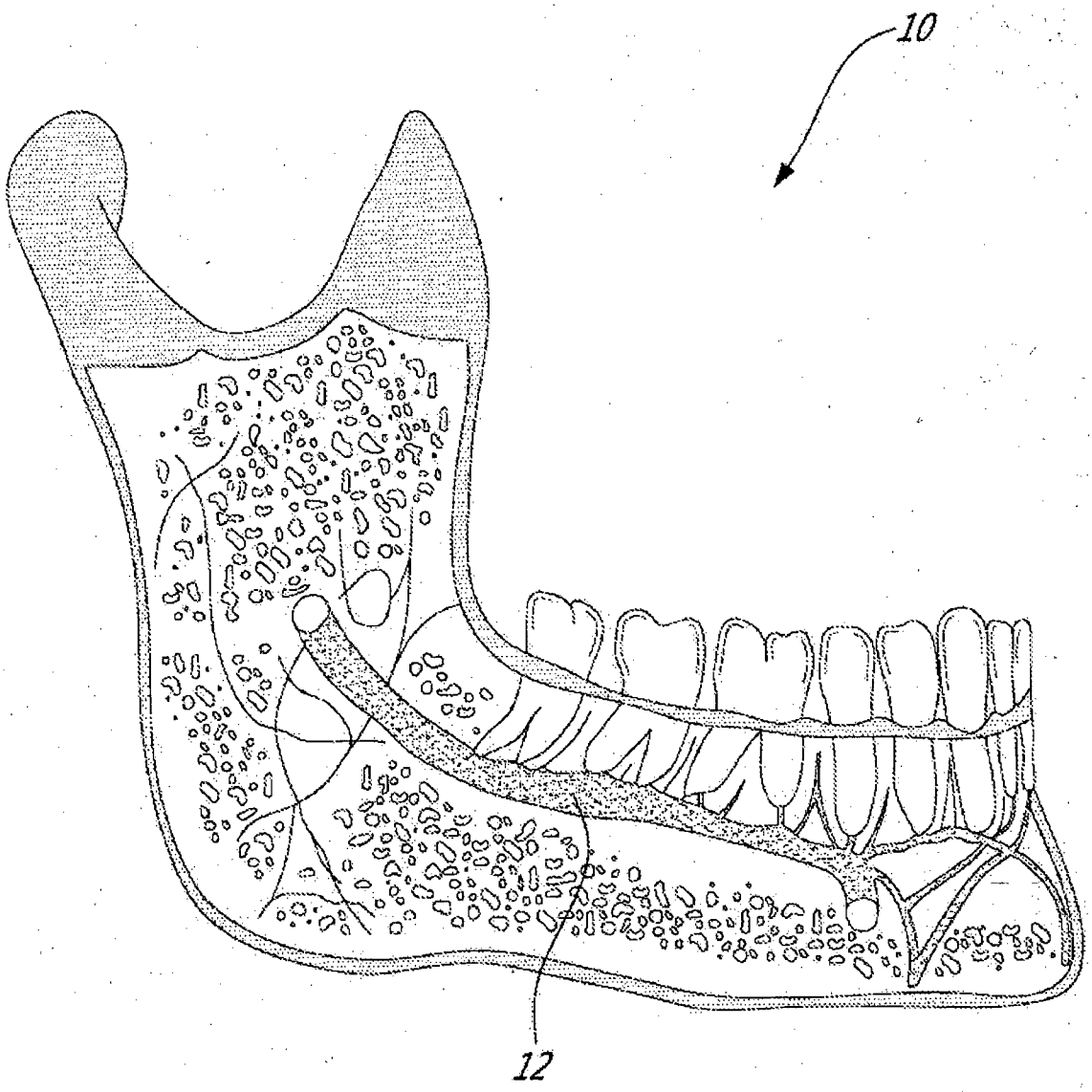

FIG. 1

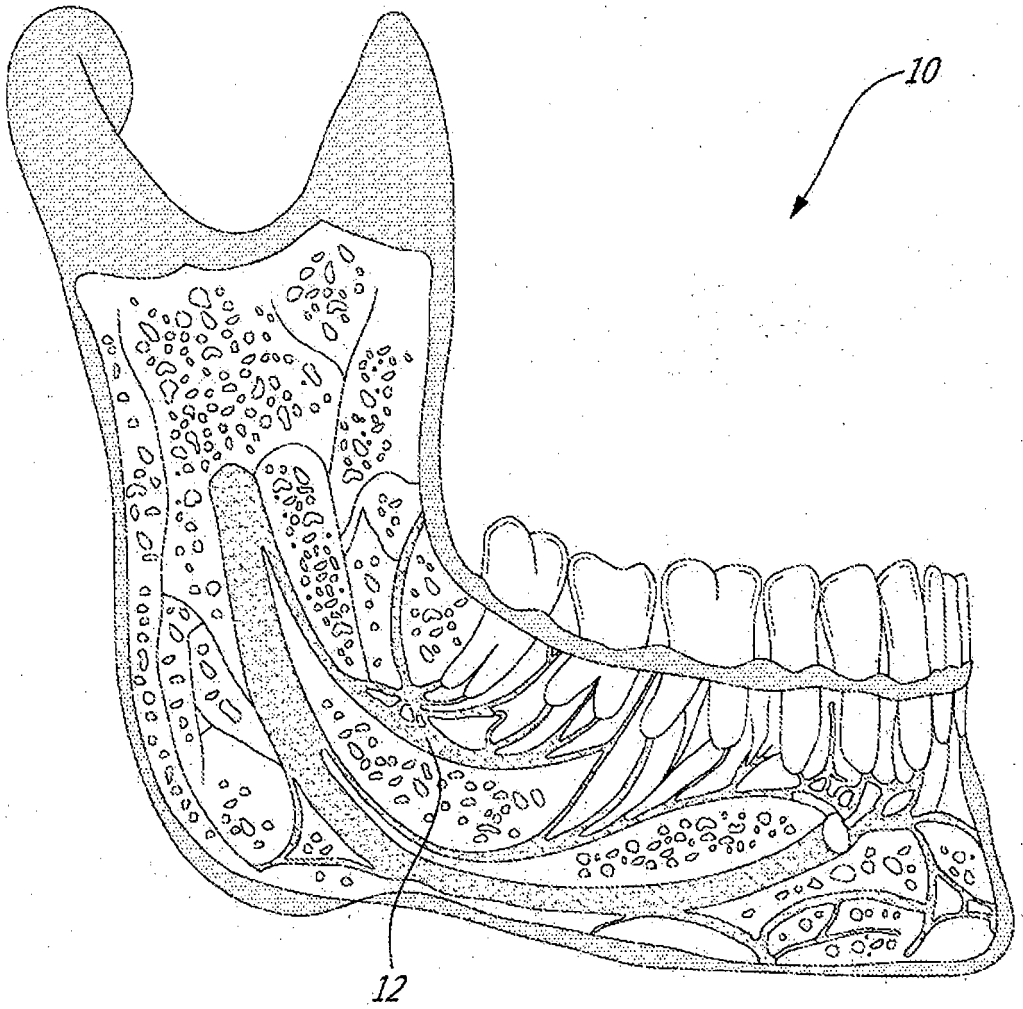

FIG. 2

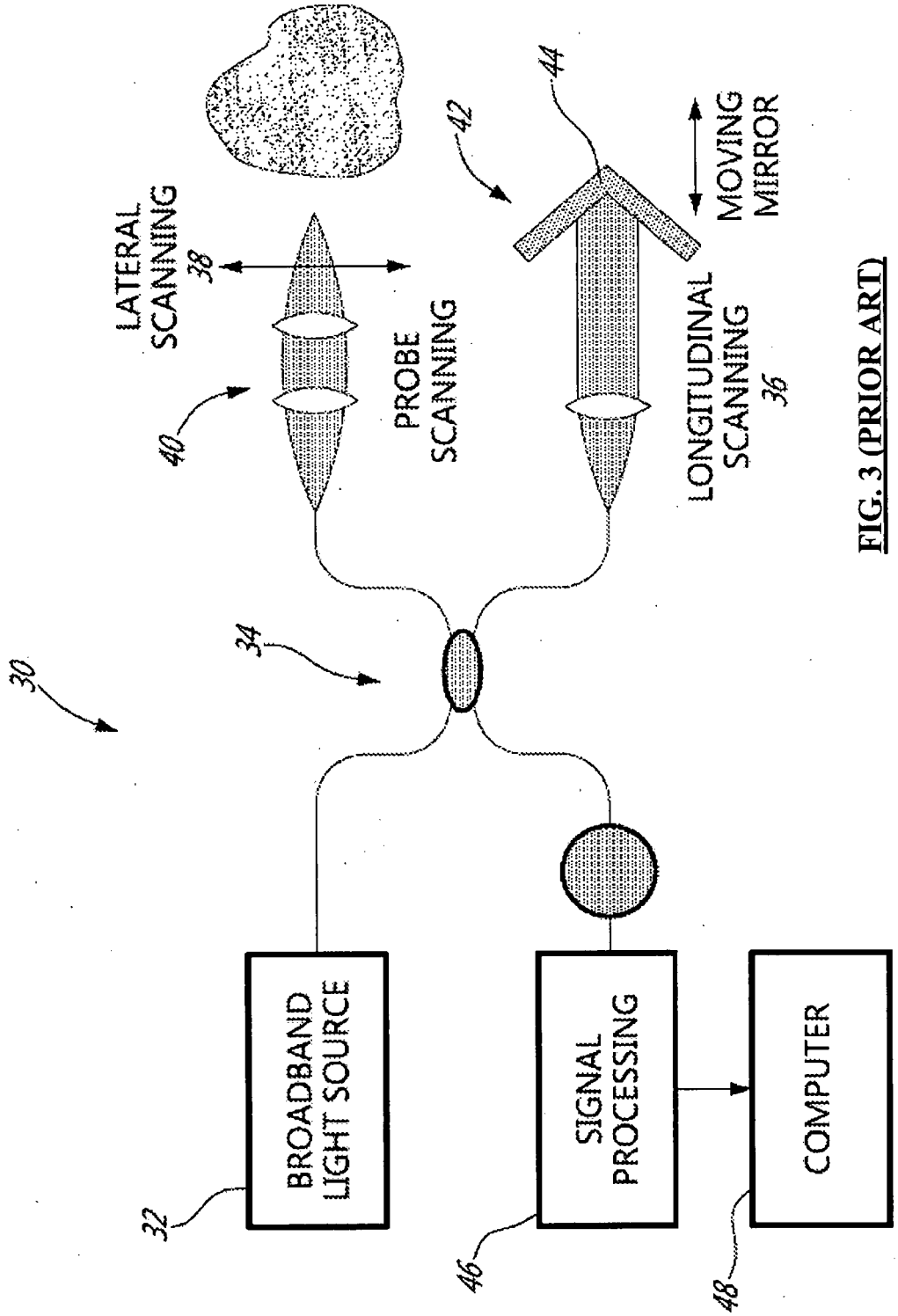

FIG. 3 (PRIOR ART)

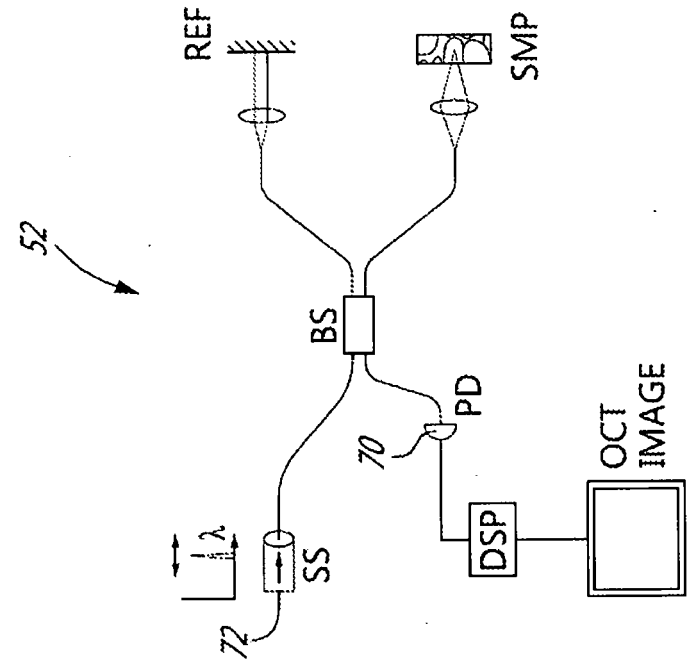

FIG. 4B (PRIOR ART)

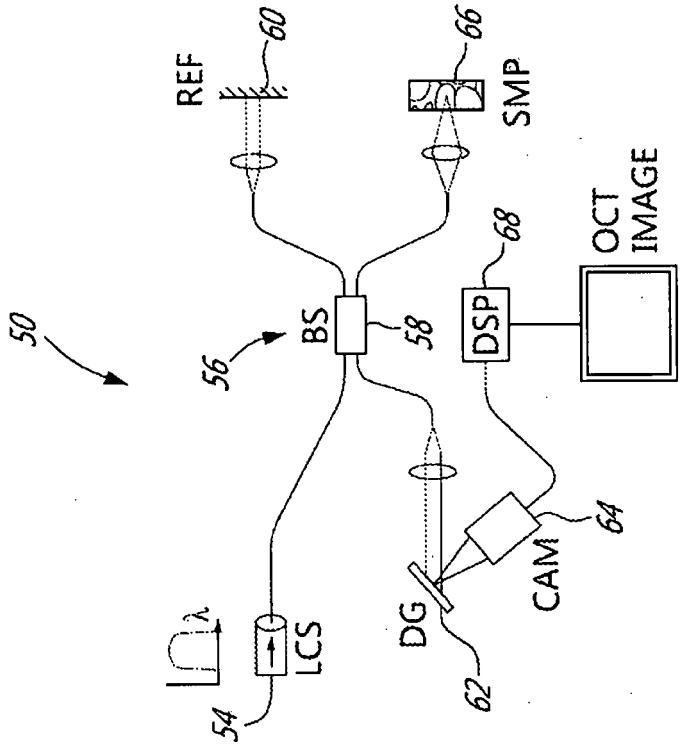

FIG. 4A (PRIOR ART)

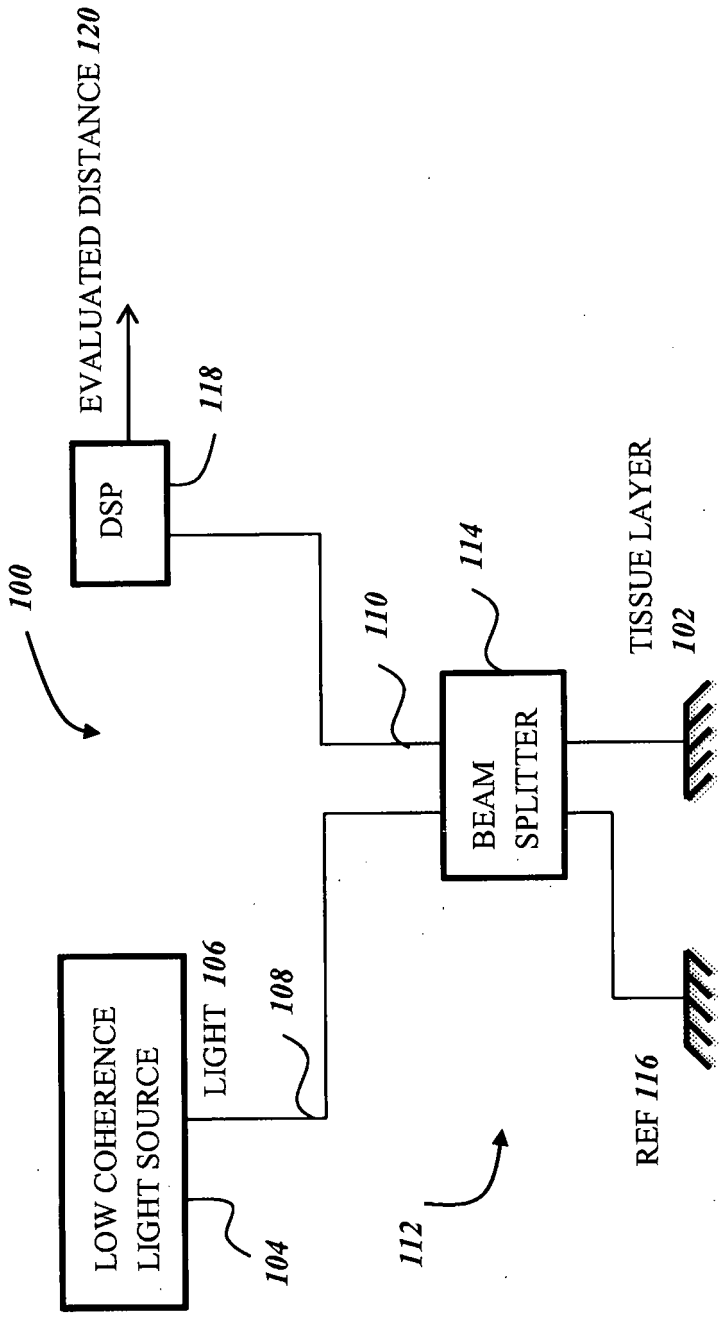
EVALUATED DISTANCE 120
DSP
118
100
110
114
TISSUE LAYER
102
BEAM SPLITTER
LOW COHERENCE LIGHT SOURCE
LIGHT 106
108
104
112
REF 116

FIG. 5

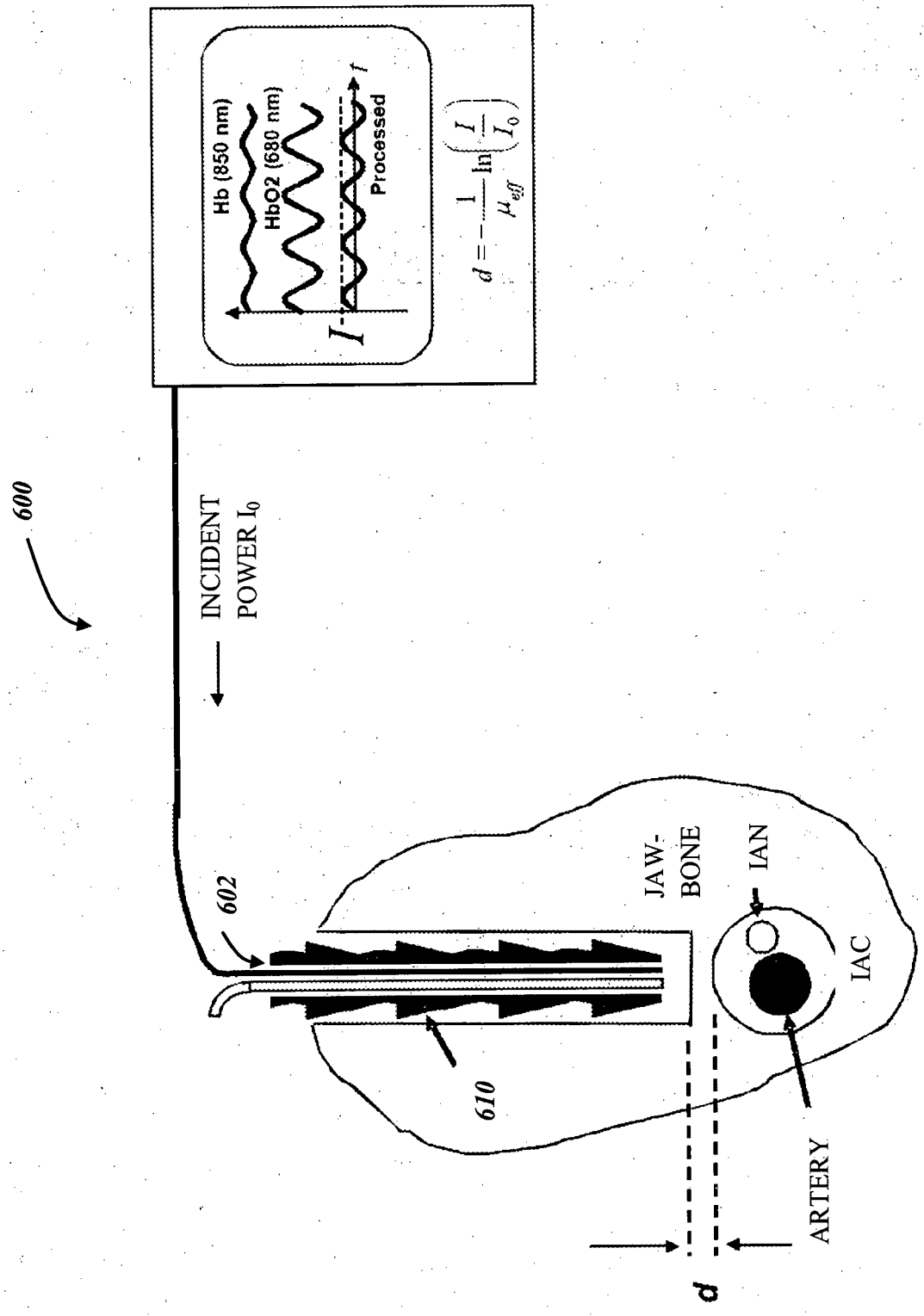
600
INCIDENT
POWER I_0
602
610
JAW-
BONE
IAN
IAC
ARTERY
d
Hb (850 nm)
HbO2 (680 nm)
Processed
I
t
$d = -\frac{1}{\mu_{eff}} \ln\left(\frac{I}{I_0}\right)$

FIG. 6

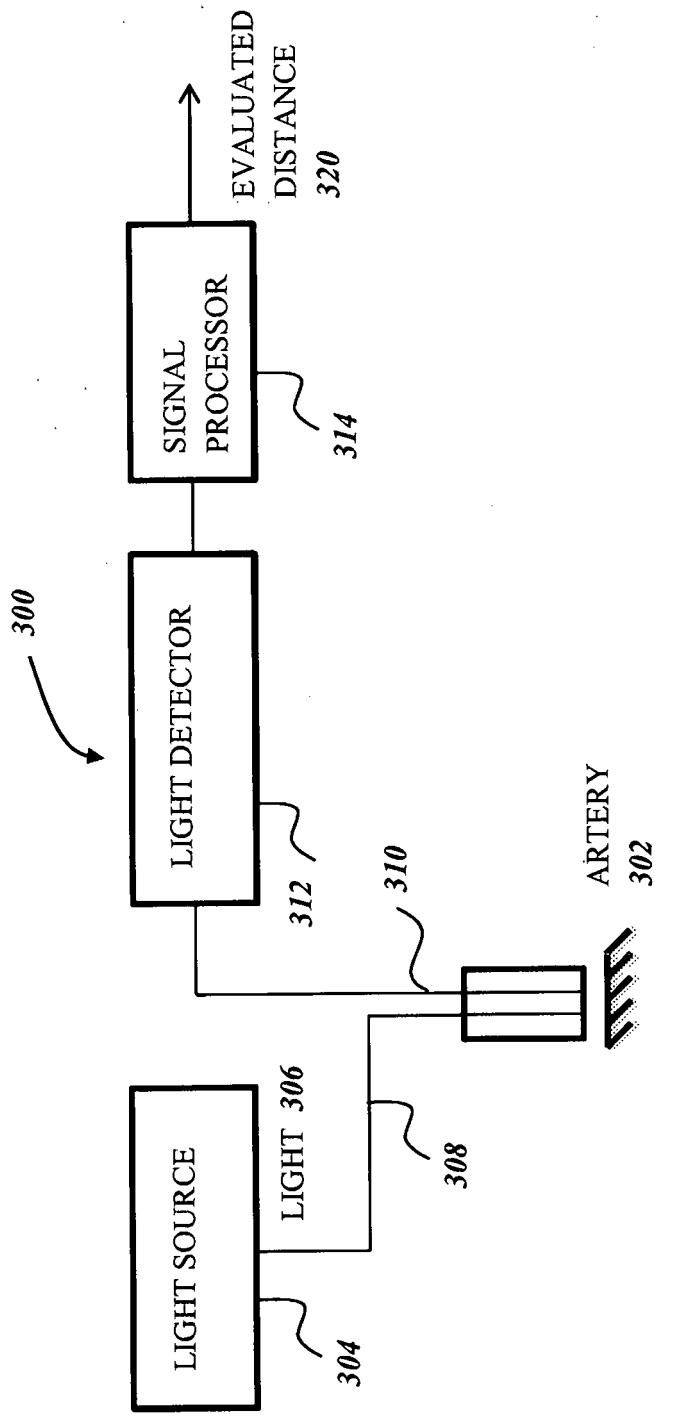
300
LIGHT SOURCE
304
LIGHT 306
308
LIGHT DETECTOR
312
310
ARTERY
302
SIGNAL PROCESSOR
314
EVALUATED DISTANCE
320

FIG. 7

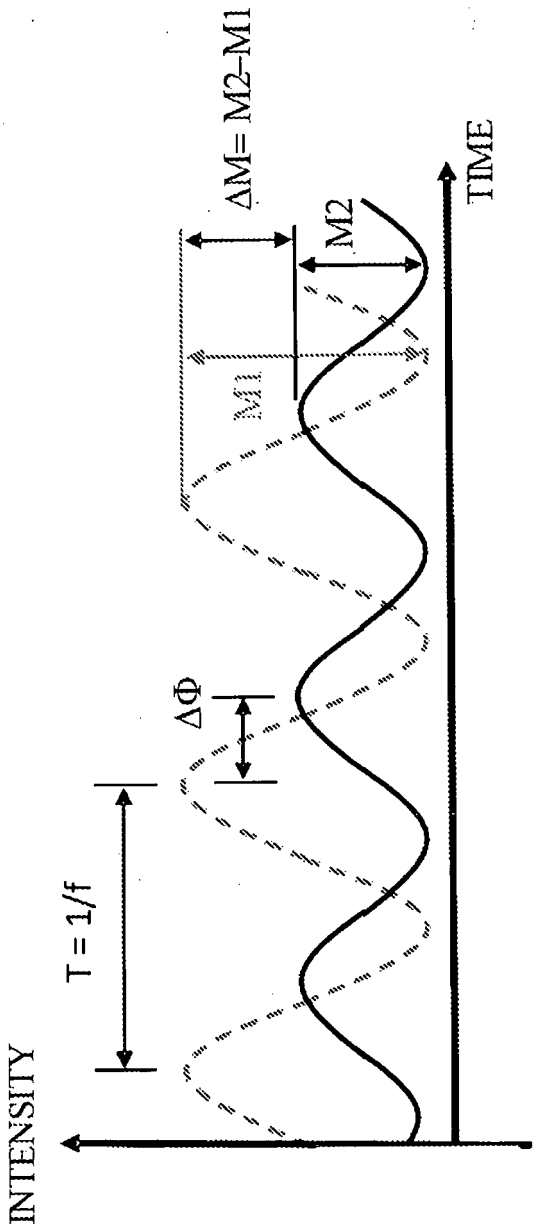

FIG. 8

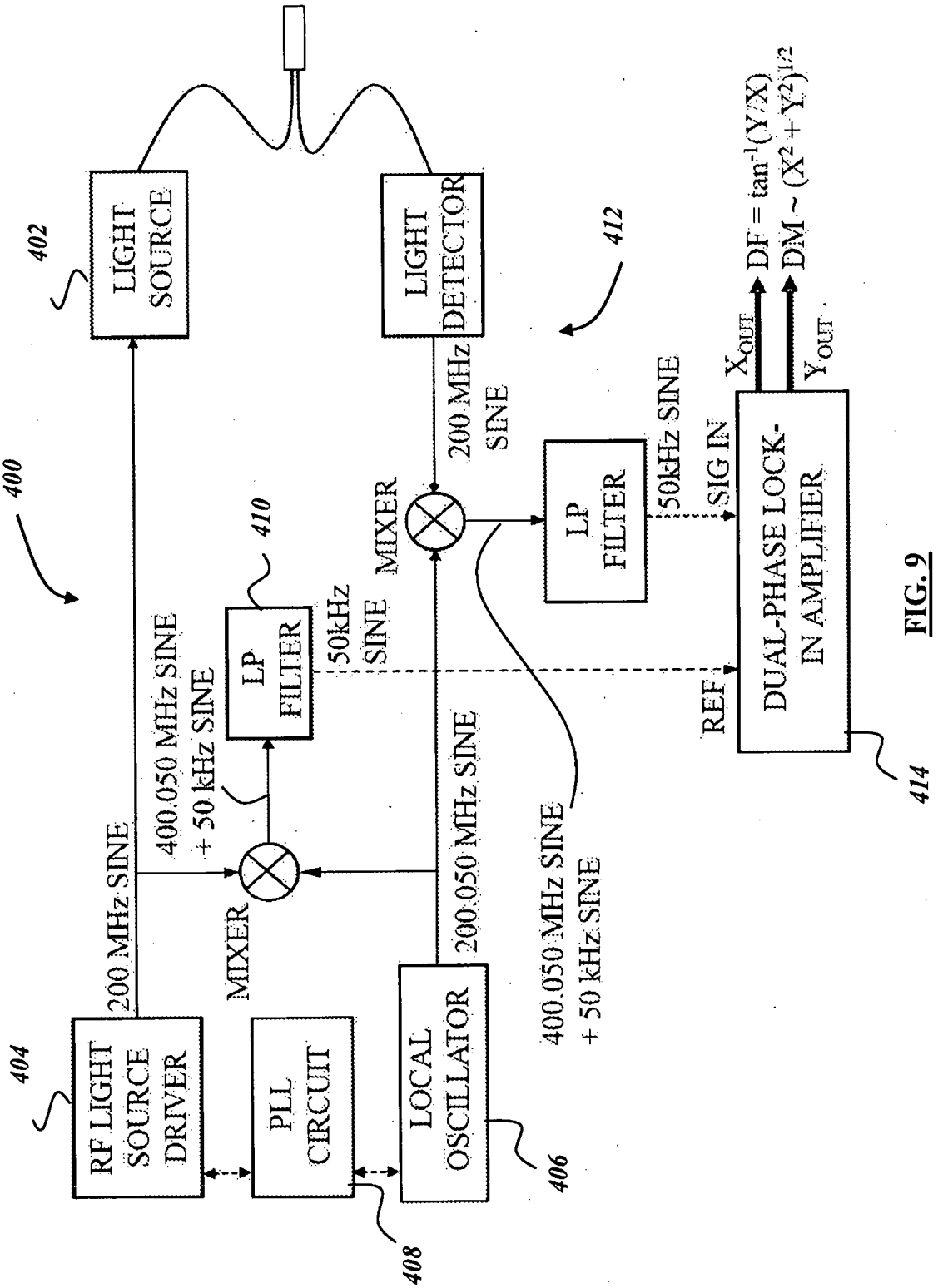
400
402
LIGHT SOURCE
LIGHT DETECTOR
412
200 MHz SINE
MIXER
LP FILTER
50kHz SINE
SIG IN
X_{OUT} $DF = \tan^{-1}(Y/X)$
Y_{OUT} $DM \sim (X^2 + Y^2)^{1/2}$
DUAL-PHASE LOCK-IN AMPLIFIER
REF
414
410
LP FILTER
50kHz SINE
400.050 MHz SINE + 50 kHz SINE
MIXER
200 MHz SINE
200.050 MHz SINE
400.050 MHz SINE + 50 kHz SINE
404
RF LIGHT SOURCE DRIVER
PLL CIRCUIT
LOCAL OSCILLATOR
406
408

FIG. 9

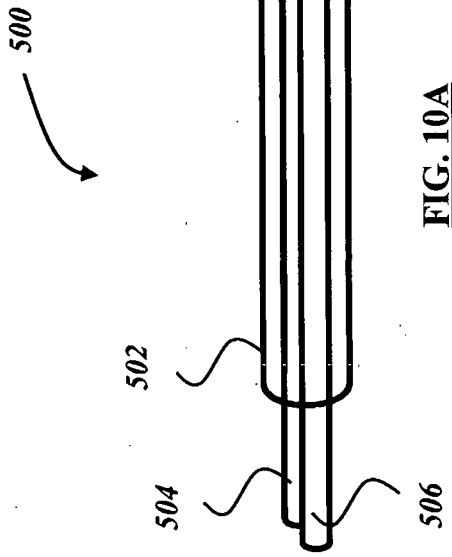

FIG. 10A

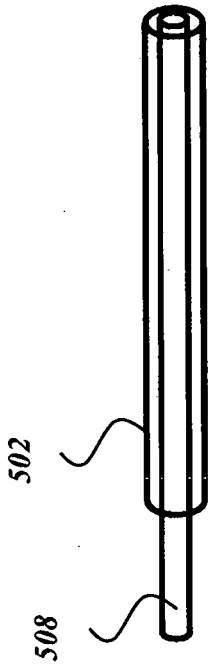

FIG. 10B

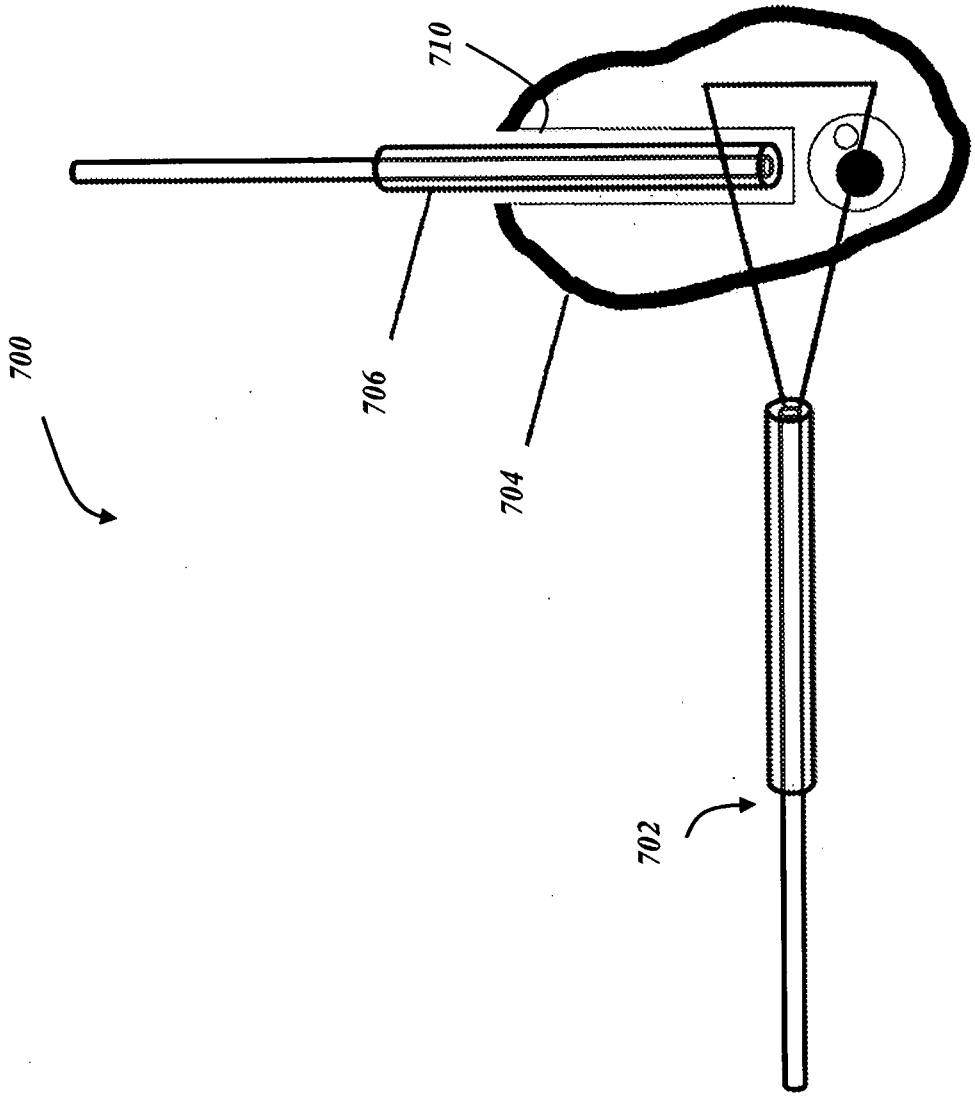

FIG. 11

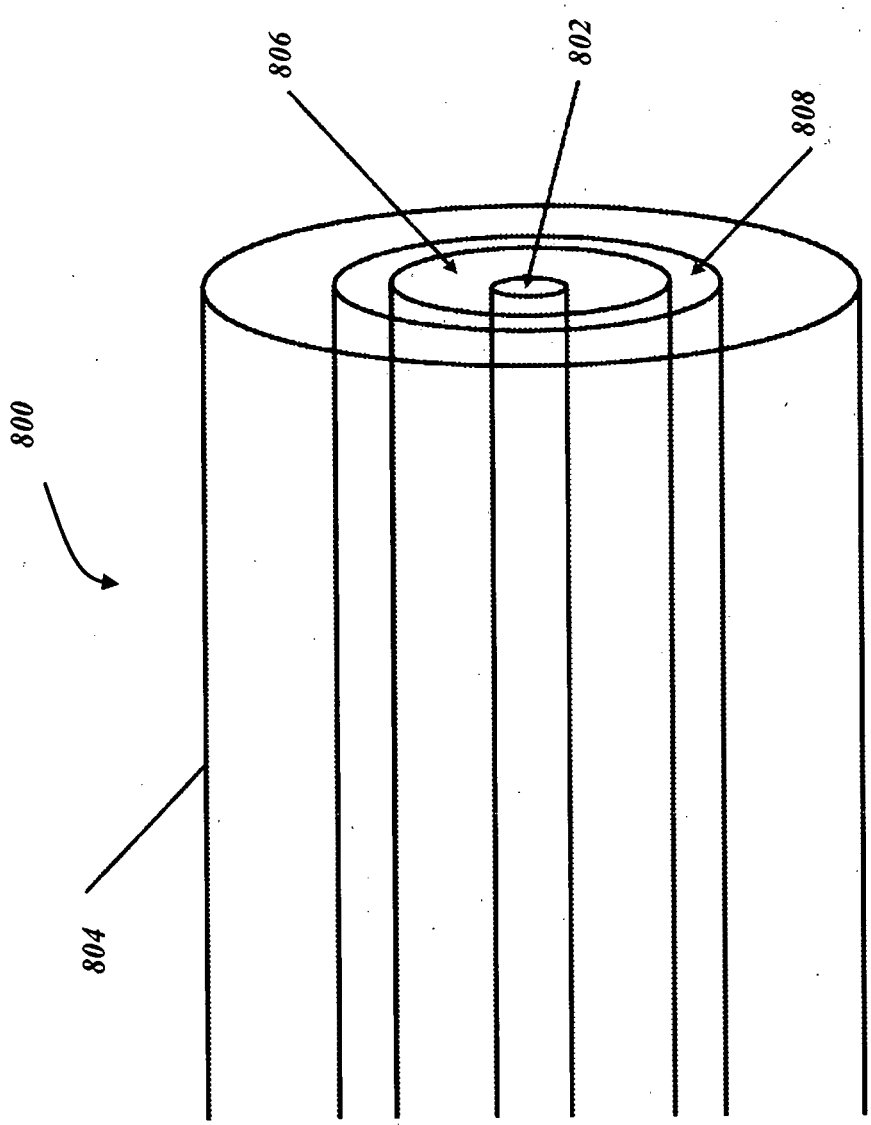

FIG. 12

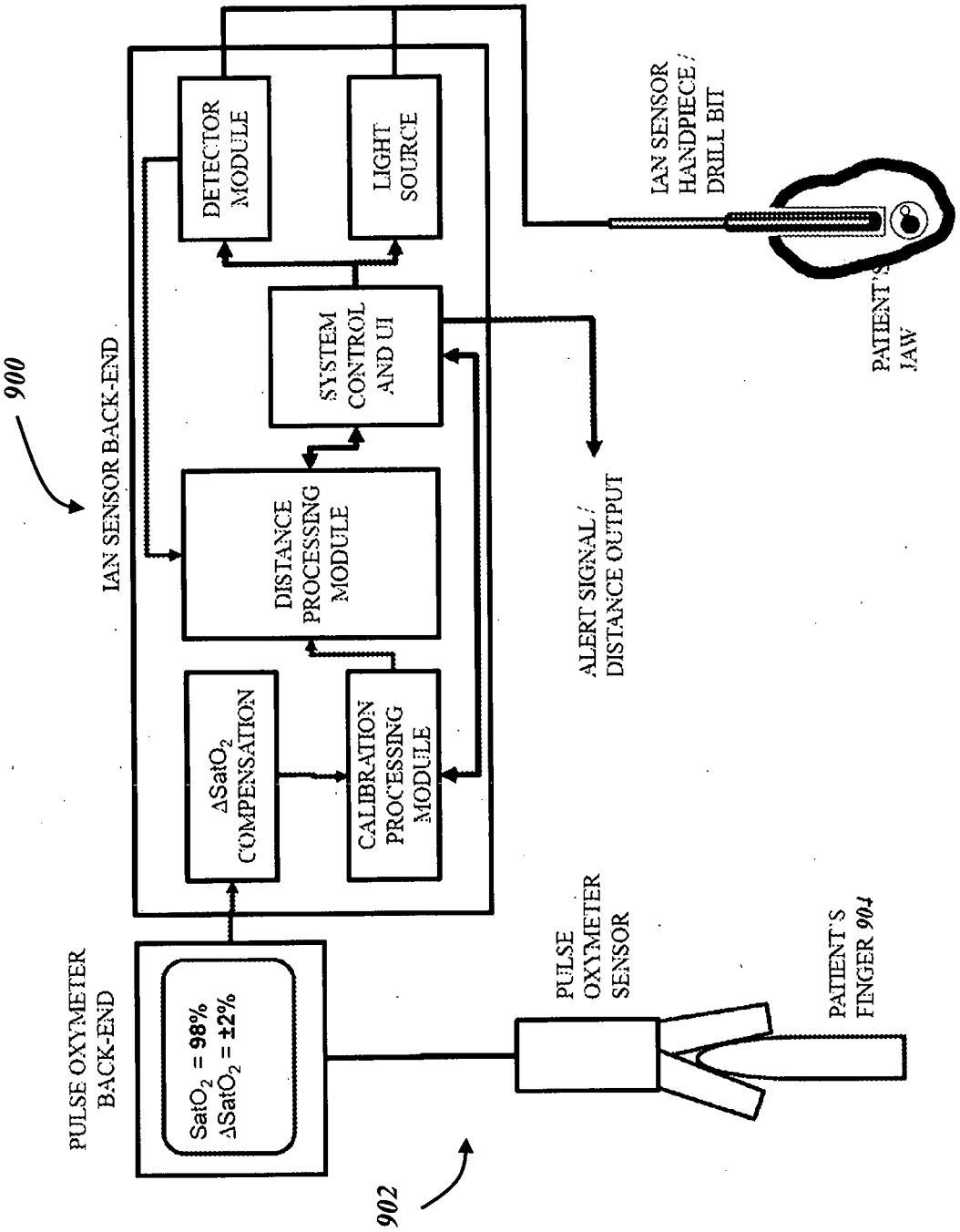
900
IAN SENSOR BACK-END
DETECTOR MODULE
LIGHT SOURCE
SYSTEM CONTROL AND UI
DISTANCE PROCESSING MODULE
ΔSatO2 COMPENSATION
CALIBRATION PROCESSING MODULE
ALERT SIGNAL / DISTANCE OUTPUT
IAN SENSOR HANDPIECE / DRILL BIT
PATIENT'S JAW
PULSE OXYMETER BACK-END
SatO2 = 98%
ΔSatO2 = ±2%
PULSE OXYMETER SENSOR
PATIENT'S FINGER 904
902

FIG. 13

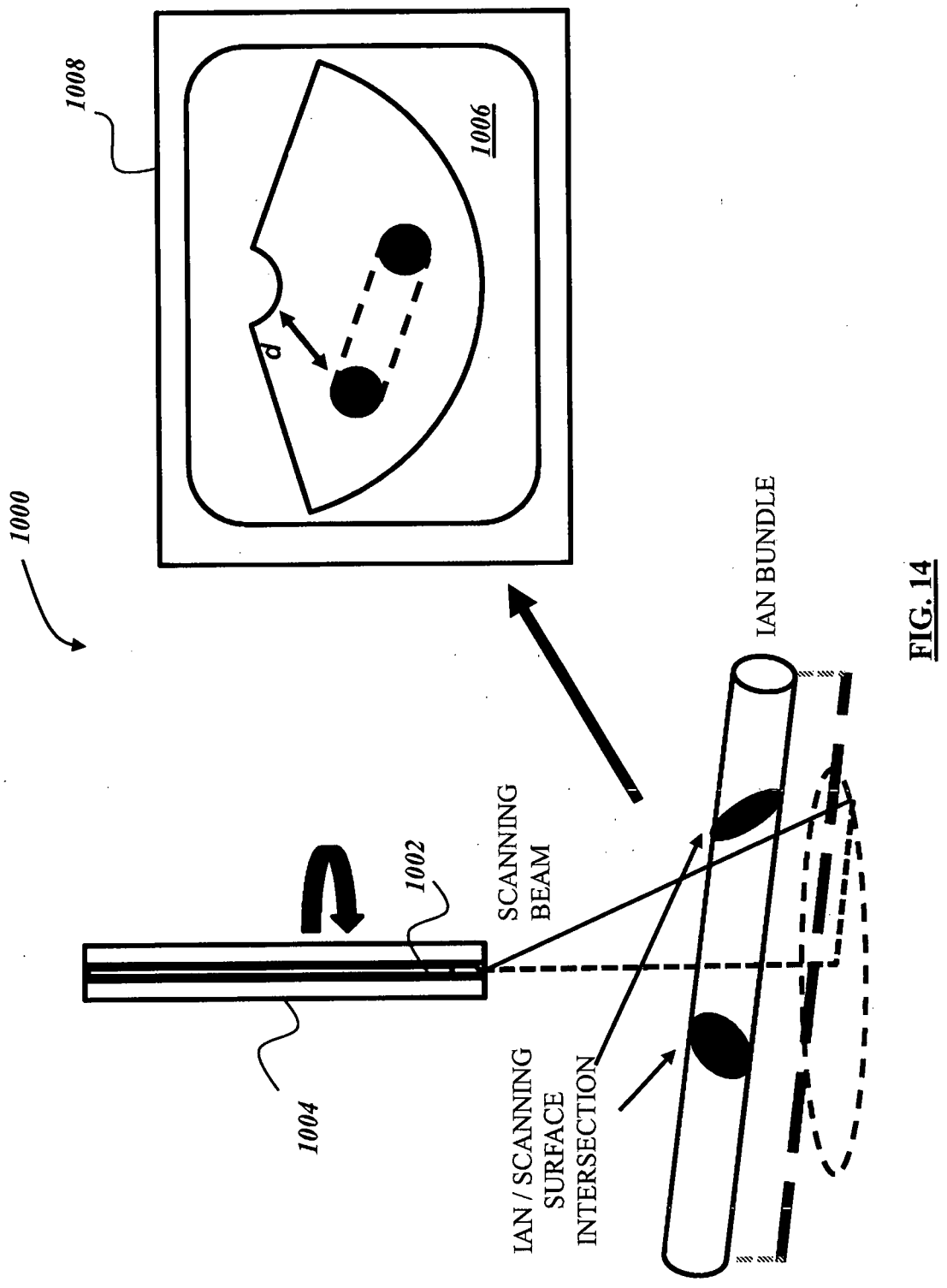
1000
1008
1006
d
IAN BUNDLE
SCANNING BEAM
1002
1004
IAN / SCANNING SURFACE INTERSECTION

FIG. 14

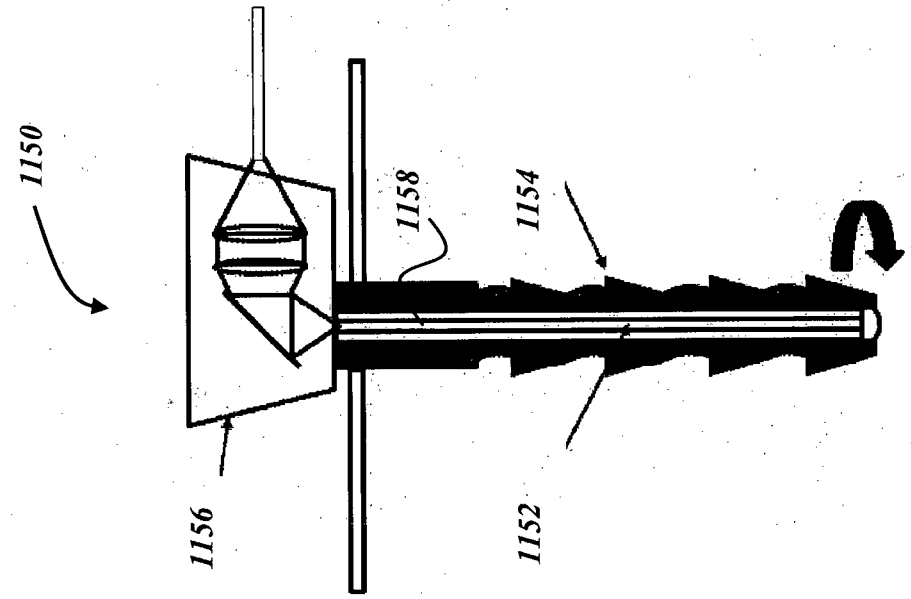

FIG. 15B

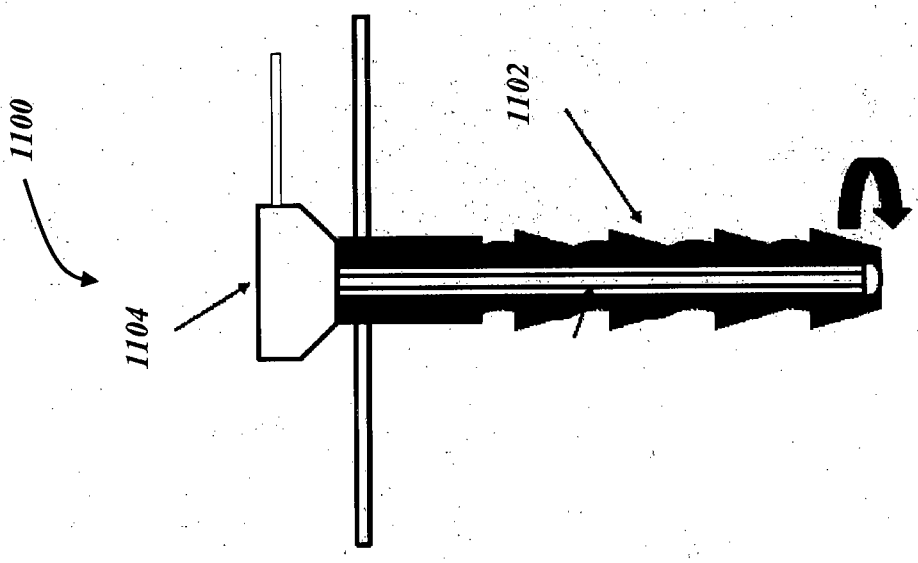

FIG. 15A

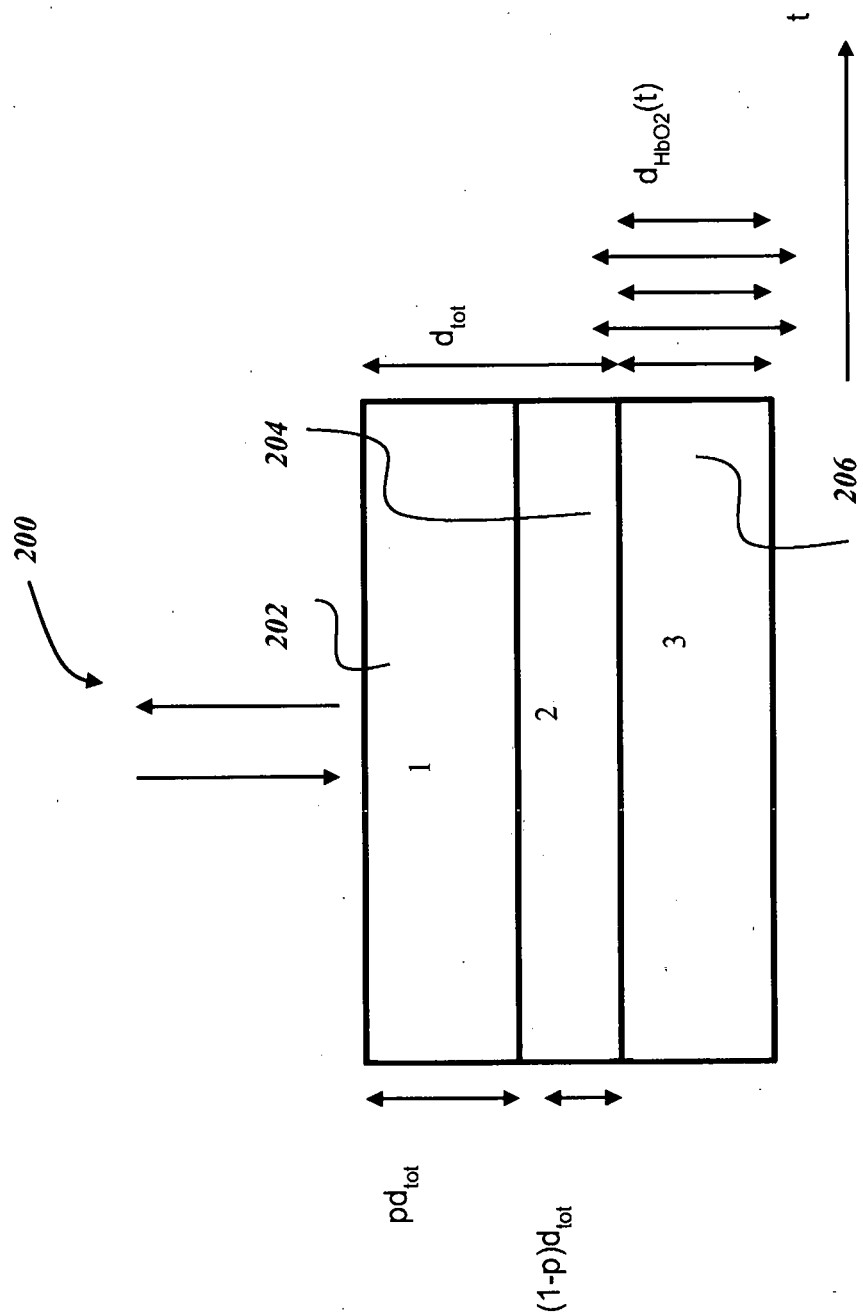

FIG. 16

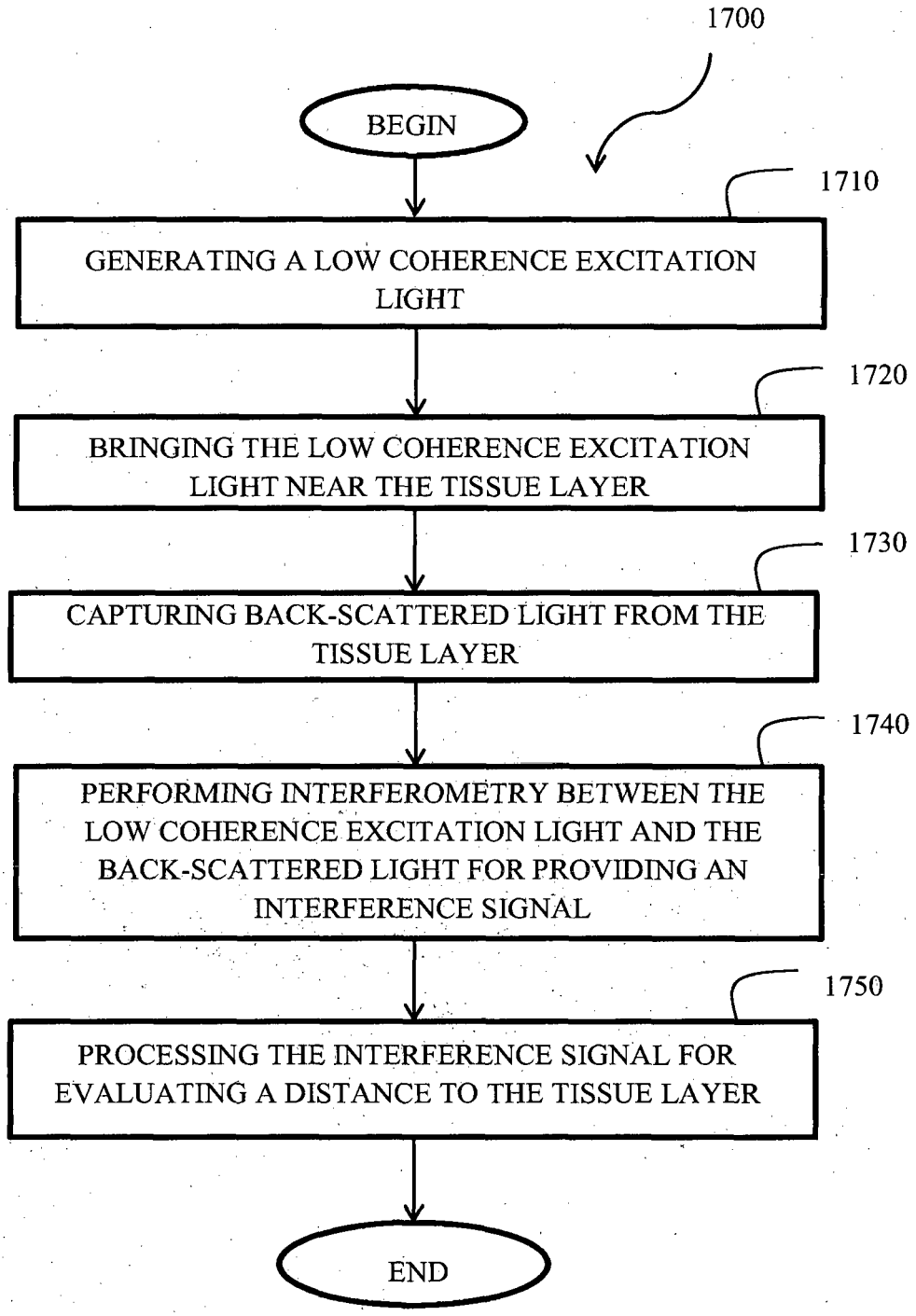
1700
BEGIN
1710
GENERATING A LOW COHERENCE EXCITATION LIGHT
1720
BRINGING THE LOW COHERENCE EXCITATION LIGHT NEAR THE TISSUE LAYER
1730
CAPTURING BACK-SCATTERED LIGHT FROM THE TISSUE LAYER
1740
PERFORMING INTERFEROMETRY BETWEEN THE LOW COHERENCE EXCITATION LIGHT AND THE BACK-SCATTERED LIGHT FOR PROVIDING AN INTERFERENCE SIGNAL
1750
PROCESSING THE INTERFERENCE SIGNAL FOR EVALUATING A DISTANCE TO THE TISSUE LAYER
END

FIG. 17

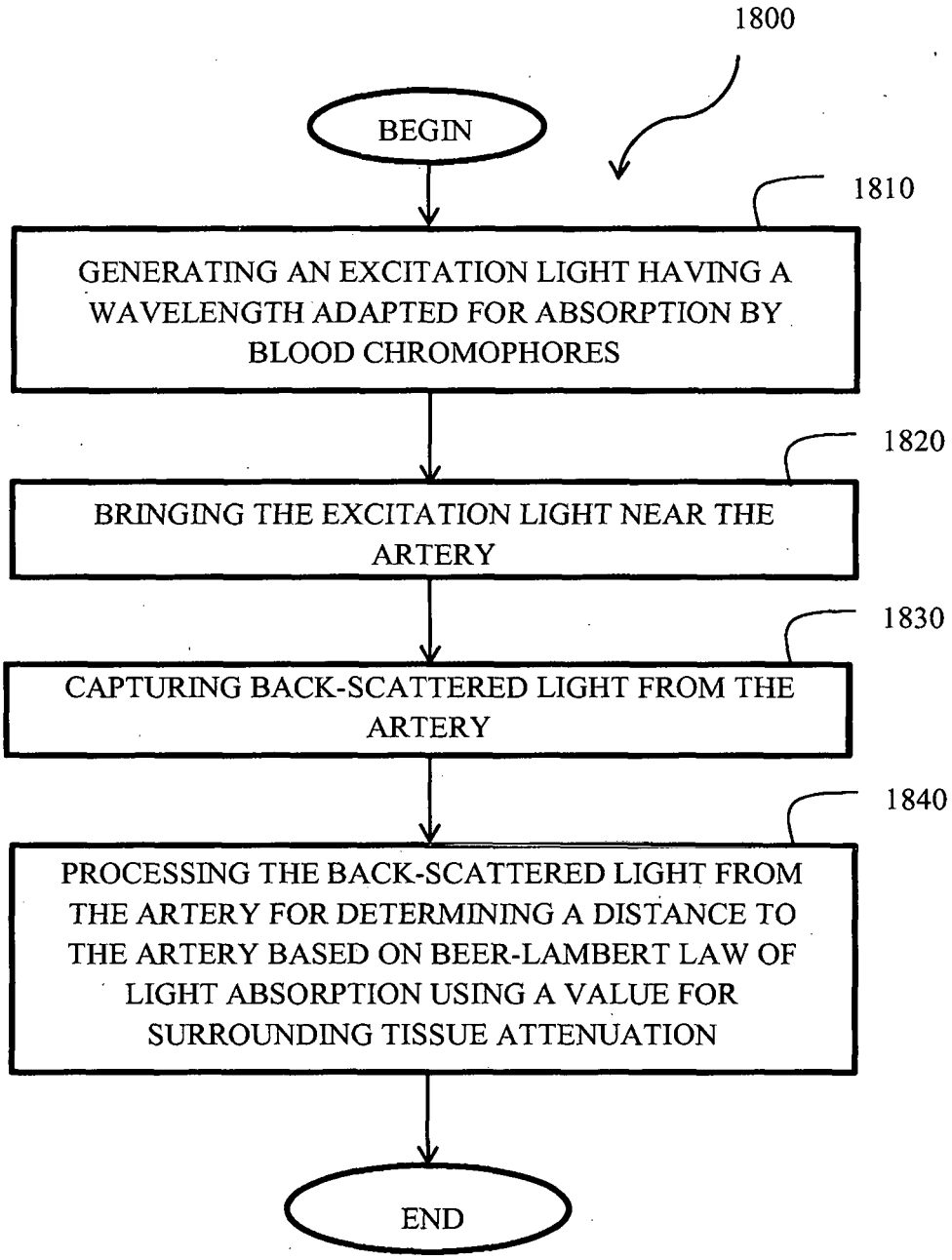
1800
BEGIN
1810
GENERATING AN EXCITATION LIGHT HAVING A WAVELENGTH ADAPTED FOR ABSORPTION BY BLOOD CHROMOPHORES
1820
BRINGING THE EXCITATION LIGHT NEAR THE ARTERY
1830
CAPTURING BACK-SCATTERED LIGHT FROM THE ARTERY
1840
PROCESSING THE BACK-SCATTERED LIGHT FROM THE ARTERY FOR DETERMINING A DISTANCE TO THE ARTERY BASED ON BEER-LAMBERT LAW OF LIGHT ABSORPTION USING A VALUE FOR SURROUNDING TISSUE ATTENUATION
END

FIG. 18

REFERENCES CITED IN THE DESCRIPTION

This list of references cited by the applicant is for the reader's convenience only. It does not form part of the European patent document. Even though great care has been taken in compiling the references, errors or omissions cannot be excluded and the EPO disclaims all liability in this regard.

Patent documents cited in the description

- US 61477787 A **[0001]**
- US 32955711 A **[0001]**
- US 20060285635 A1 **[0008]**
- US 6419484 B1 **[0009]**

Non-patent literature cited in the description

- **MISCH ; RESNIK.** *Implant Dentistry,* 2010, vol. 19, 378-386 **[0006]**
- **C.D. MORRIS et al.** *J. Oral Maxillo. Surg.,* 2010, vol. 68, 2833-2836 **[0013]**
- **ONG, F.R. ; BOUAZZA-MAROUF, K.** The detection of drill bit break-through for the enhancement of safety in mechatronic assisted orthopaedic drilling. *MECHATRONICS,* 1999, vol. 9, 565-588 **[0020]**
- **A. MARIAMPILLAI et al.** *Opt. Lett.,* 2008, vol. 33 (13), 1530 **[0054]**
- **A. MARIAMPILLAI et al.** *Opt. Lett.,* 2010, vol. 35 (8), 1257 **[0054]**

专利名称(译)	用于光学评估原位接近下牙槽神经的系统		
公开(公告)号	EP2699165B1	公开(公告)日	2017-06-07
申请号	EP2012774529	申请日	2012-01-04
[标]申请(专利权)人(译)	该ghaderi哈桑博士		
申请(专利权)人(译)	原因之一，HASSAN GHADERI博士		
当前申请(专利权)人(译)	活的Vue公司		
[标]发明人	MOGHADDAM HASSAN GHADERI GALLANT PASCAL MERMUT OZZY VEILLEUX ISRAEL		
发明人	MOGHADDAM, HASSAN, GHADERI GALLANT, PASCAL MERMUT, OZZY VEILLEUX, ISRAËL		
IPC分类号	A61B5/026 A61B17/16 A61B17/17 A61C1/08 A61B5/00 A61C19/04 A61C8/00 A61B5/1455		
CPC分类号	A61B17/1703 A61B5/0066 A61B5/0075 A61B5/0261 A61B5/14551 A61B5/4542 A61B5/489 A61B5/4893 A61B17/1673 A61B2034/2057 A61B2090/306 A61C1/084 A61C1/088 A61C8/0089 A61C19/04		
代理机构(译)	LAVOIX		
优先权	61/477787 2011-04-21 US 13/329557 2011-12-19 US		
其他公开文献	EP2699165A4 EP2699165A1		
外部链接	Espacenet		

摘要(译)

一种用于在钻探过程中确定手术钻头与动脉的接近度的手术钻探系统，包括光谱吸收探针的激发和/或收集光学通道，其中所述激发通道提供被配置为被血生色团吸收和收集的光 通道捕获由所述动脉调制的散射的反向散射光； 光探测器； 信号处理器，用于基于所述反向散射光确定组织与探针之间的距离。 一种在钻孔过程中确定外科手术钻头与动脉的接近度的过程，包括：将所述激发光带到包括动脉的组织附近； 捕获来自所述组织的散射的反向散射光； 检测由所述血流动力学调制的所述光，所述光包括与所述周期性变化有关的振荡信号； 处理所述光并确定手术钻头与动脉的接近度。